Elsevier Editorial System(tm) for Energy Conversion and Management
Manuscript Draft

Manuscript Number:

Title: Performance analysis and optimization of a combined cooling and power system using low boiling point working fluid driven by engine waste heat

Article Type: Original research paper

Section/Category: 1. Energy Conservation and Efficient Utilization

Keywords: Internal combustion engine; Brayton cycle; Waste heat recovery; Dual-pressure organic Rankine cycle; Ejector refrigeration cycle; Optimization

Corresponding Author: Dr. Jiangfeng Wang, Ph.D.

Corresponding Author's Institution: Xi'an Jiaotong University

First Author: Wenge Huang

Order of Authors: Wenge Huang; Jiangfeng Wang, Ph.D.; Jiaxi Xia; Pan Zhao, Ph.D.; Yiping Dai

Abstract: This paper develops a combined cooling and power system to recover waste heat from exhaust gas and jacket water in internal combustion engines using low boiling point fluid as working fluid. The system consists of a CO2 Brayton cycle (CBC), a dual-pressure organic Rankine cycle (DORC) and an ejector refrigeration cycle (ERC). Comprehensive thermodynamic and exergoeconomic models of the system are performed and seven key parameters are selected to analyze the system performance. To obtain a better performance of the system, single-objective optimization is carried out by means of genetic algorithm with system product levelized exergy cost as the objective function. Results show that the increase of the BC turbine inlet temperature and inlet pressure can cause the increase of the system net power output. In both the high-pressure side and low-pressure side of the DORC, the increase of the ORC turbine inlet temperature causes the increase of the levelized exergy cost while the increase of the ORC turbine inlet pressure does the opposite. The increase of the ejector primary inlet pressure causes the increase of system capital cost. Optimization shows that minimum levelized exergy cost for system product is 53.25 $ (MWh)-1 with exergy efficiency of 37.31%.

Suggested Reviewers: Kamel Hooman
University of Qeensland
k.hooman@uq.edu.au

Weifeng He
wfhe@nuaa.edu.cn

Zhixin Sun
zxsun@fzu.edu.cn

*Cover letter

Dear Editor:

We are sending a manuscript entitled “Performance analysis and optimization of a combined cooling and power system using low boiling point working fluid driven by engine waste heat”, which we should like to submit for publication in Energy Conversion and Management. We investigate a combined cooling and power system driven by exhaust gas and jacket water from an internal combustion engine. The mathematical model of the system is established to simulate the cycles under steady-state conditions. A parametric analysis of seven key parameters is conducted to examine their effects on the thermodynamic and exergoeconomic performance of the system. An optimization is conducted by genetic algorithm to obtain better system performance.

We declare that the manuscript has not been previously published, is not currently submitted for review to any other journal and will not be submitted elsewhere before one decision is made. Its publication is approved by all authors. If accepted, it will not be published elsewhere in the same form, in English or in any other language.

We appreciate your consideration of our manuscript, and we look forward to receiving comments from the reviewers.

Sincerely,

Jiangfeng Wang (on behalf of the authors’ team)

Institute of Turbomachinery

Cover letter

Shaanxi Engineering Laboratory of Turbomachinery and Power Equipment

State Key Laboratory of Multiphase Flow in Power Engineering

School of Energy and Power Engineering

Xi’an Jiaotong University, Xi’an, China

Highlights

A combined cooling and power system driven by engine exhaust gas and jacket water is proposed.

Thermodynamic and exergoeconomic performance of the system are analyzed.

Optimization for the combined cooling and power system is conducted by genetic algorithm.

Performance analysis and optimization of a combined cooling and power system using low boiling point working fluid driven by engine waste heat

Wenge Huang, Jiangfeng Wang*, Jiaxi Xia, Pan Zhao, Yiping Dai

Institute of Turbomachinery, Shaanxi Engineering Laboratory of Turbomachinery and Power Equipment, State Key Laboratory of Multiphase Flow in Power Engineering, School of Energy and Power Engineering, Xi'an Jiaotong University, Xi'an 710049, China

Corresponding author: Jiangfeng Wang

Mailing address:

Institute of Turbomachinery, Shaanxi Engineering Laboratory of Turbomachinery and Power Equipment, State Key Laboratory of Multiphase Flow in Power Engineering, School of Energy and Power Engineering

Xi'an Jiaotong University, Xi'an 710049, China

E-mail address: jfwang@mail.xjtu.edu.cn (JF Wang).

Performance analysis and optimization of a combined cooling and power system using low boiling point working fluid driven by engine waste heat

Wenge Huang, Jiangfeng Wang*, Jiaxi Xia, Pan Zhao, Yiping Dai

Institute of Turbomachinery, Shaanxi Engineering Laboratory of Turbomachinery and Power Equipment, State Key Laboratory of Multiphase Flow in Power Engineering, School of Energy and Power Engineering, Xi'an Jiaotong University, Xi'an 710049, China

Abstract

This paper develops a combined cooling and power system to recover waste heat from exhaust gas and jacket water in internal combustion engines using low boiling point fluid as working fluid. The system consists of a CO_2 Brayton cycle (CBC), a dual-pressure organic Rankine cycle (DORC) and an ejector refrigeration cycle (ERC). Comprehensive thermodynamic and exergoeconomic models of the system are performed and seven key parameters are selected to analyze the system performance. To obtain a better performance of the system, single-objective optimization is carried out by means of genetic algorithm with system product levelized exergy cost as the objective function. Results show that the increase of the BC turbine inlet temperature and inlet pressure can cause the increase of the system net power output. In both the high-pressure side and low-pressure side of the DORC, the increase of the ORC turbine inlet temperature causes the increase of the levelized exergy cost while the increase of the ORC turbine inlet pressure does the opposite. The increase of the

ejector primary inlet pressure causes the increase of system capital cost. Optimization shows that minimum levelized exergy cost for system product is 53.25 \$ (MWh)$^{-1}$ with exergy efficiency of 37.31%.

Keyworks:

Internal combustion engine

Brayton cycle

Waste heat recovery

Dual-pressure organic Rankine cycle

Ejector refrigeration cycle

Optimization

Nomenclature

A	area, m^2	ρ	density, kg m^{-3}
BC	Brayton cycle	μ	dynamic viscosity, m^2 s^{-1}
B_o	boiling number	η	efficiency, %
c	average cost per unit of exergy, \$ (MWh)$^{-1}$	δ	thickness, m
c_p	specific heat, kJ kg^{-1} K^{-1}	*Subscribe*	
C	cost rate, \$ year^{-1}	1-31	state points
CBC	CO_2 Brayton cycle	g1-g3	state points
CCP	combined cooling and power	w1-w3	state points
CRF	capital recovery factor	Bt	Brayton cycle turbine
CEPCI	chemical engineering plant cost index	BM	bare module
D	diameter, m	cond	condenser

DORC	dual-pressure organic Rankine cycle	comp	compressor
e	exergy, kJ kg^{-1}	D	destruction
E	exergy flow rate, kJ s^{-1}	elec	electricity
E_{y}	exergy flow rate per year, kJ year^{-1}	es	equivalent diameter
ERC	ejector refrigeration cycle	ev	evaporation/evaporator
F	multiplying factor	ex	exergy
f	friction factor	F	fuel
G	mass flow rate, kg s^{-1}	g	exhaust gas
h	enthalpy, kJ kg^{-1}	gh	gas heater
H	depth, m	he	heat exchanger
i_{eff}	interest rate	L	loss
l	length, m	l	liquid
M	mass flow rate, kg s^{-1}	M	material
n	lifetime, year	Ot	ORC turbine
Nu	Nusselt number	P	product
P	pressure, MPa	p1	pump 1
Pr	Prandtl number	p2	pump 2
Pt	center distance between tubes, m	p3	pump 3
P_r	reduced pressure	p4	pump 4
Q	heat transfer rate, kW	pf	primary flow
Q_{cool}	cooling capacity, kW	prec	precooler
q_{m}	average imposed wall heat flux, W m^{-2}	preh	preheater

r_f	enthalpy of vaporization, kJ kg^{-1}	s	shell
T	temperature, K	t	tube
U	overall heat transfer coefficient, W m^{-2} K^{-1}	th	thermal
W	power, kW	turb	turbine
W_y	annually power, MWh year^{-1}	vg	vapor generator
x	vapor quality	w	tube wall
Z	annually levelized cost value, $ year^{-1}		
z	capital cost, K$		
Greek symbol			
α	convection heat transfer coefficient, W m^{-2} K^{-1}		
λ	heat conductivity, W m^{-1} K^{-1}		

1. Introduction

Nowadays, internal combustion engines (ICEs) are the major motive power source in energy field. ICEs are used widely in transport, construction, agriculture, etc. Over 50% of the total transportation fuel is consumed by internal combustion engines. In a typical ICE, only 30-45% of the fuel energy is converted into effective power output, while the remaining energy is discharged to environment via exhaust gas, jacket water and other means, including charge air and lubrication [1]. Thus, technologies utilizing waste heat from ICEs have been investigated by a number of researchers.

Compared to other methods, organic Rankine cycle (ORC) is recognized as a well proven and highly efficient waste heat recovery technology [2,3]. Coupling the ORC with the internal combustion engines is getting increasing interest of researchers. A volume of work was conducted to examine the potential of waste heat recovery from ICE with the help of ORC. Kalyan et al. [4] designed a system using ORC to generate power from exhaust gas in a low temperature combustion engine. Wei et al. [5] integrated an ORC system with a heavy-duty diesel engine to recover the waste heat. Srinivasan et al. [6] designed an ORC waste heat recovery system to improve the efficiency of the gas engine. Tian et al. [7] designed an ORC power generation system using engine exhaust gas as heat source.

Attention was mainly focused on the exhaust gas when people explored waste heat recovery from ICEs at early stage. ORC-based waste recovery systems mentioned above only absorbed heat from engine exhaust gas. However, there is a large amount energy exists in engine jacket water for its large mass flow rate and relatively high temperature (about 90℃). ORC-based power generation systems absorbed heat both form exhaust gas and jacket water were introduced by researchers. Vaja and Gambarotta [8] examined three different ORC cycles including a simply cycle, a preheating cycle and a regenerative cycle. Cycle preheated by jacket water was able to increase the system efficiency by about 12.5%. Rosset et al. [9] compared different ORC cycle configurations which converted waste heat from exhaust gas, from jacket water and from both. Calculation results revealed that the dual-source cycle provided the highest net power output.

To achieve a better performance for the waste heat recovery system, many studies try to improve the configurations of ORCs. Zhang et al. [10] developed a novel system driven by waste heat in an ICE with a dual-loop ORC. The high-temperature cycle absorbed heat from the exhaust gas and the low-temperature cycle recovered heat from the high-temperature cycle and the jacket water. Yang et al. [11] modeled a dual-loop ORC system driven by waste heat in ICE. High-temperature cycle absorbed heat from the exhaust gas and low-temperature cycle absorbed heat from secondary exhaust gas and the jacket water. Ge et al. [12] designed a dual-loop ORC system to recover waste heat using different working fluids. Zeotropic mixture was used to recover high-temperature exhaust gas and R600a/R601a mixture was used to absorb heat in low-temperature jacket water. Systems integrated with complicated organic Rankine cycles were developed by many researchers [13-15].

Thermal stability of the organic working fluid should be considered when developing organic Rankine cycles to recovery waste heat from engine exhaust gas. Organic-based fluids would decompose under high-temperature and high-pressure conditions [16]. The low decomposition temperature of organic working fluid in ORC is about 200-300℃ while the temperature of engine exhaust gas can be more than 500℃. For all the studies mentioned above, the organic working fluid absorbs heat directly form the high-temperature exhaust gas, causing the potential of working fluid decomposition. Though an intermediate loop with thermal oil can be added between the ORC and the exhaust gas to avoid the decomposition [17,18], a large amount of high-temperature waste heat is not utilized at all. In order to solve this issue, researchers placed other waste heat recovery system between the ORC and exhaust gas to exploit to high-temperature waste heat. Thermoelectric generator (TEG), for example, was introduced by Miller et al. [19] to the utilize the high temperature waste heat in exhaust gas. After the TEG process, the cooled exhaust gas could drive the ORC safely. However, because of the low energy conversion capacity of the TEG, power generated by the TEG was much smaller than the ORC in the same system [20]. Shu et al. [21] placed a steam Rankine cycle between ORC and exhaust gas for waste heat recovery from the gas engines. The steam Rankine cycle was the topping cycle to recovery heat from the high-temperature exhaust gas and organic Rankine cycle was the bottoming cycle to recovery heat from the exhaust water vapor. Large power output was provided by both the steam Rankine cycle and the ORC in the system. However, steam in the steam Rankine cycle requires a large superheated degree, or it may condense during the expansion and damage the turbine blades. As a result, structure of the steam Rankine cycle turbine is complex. Brayton cycle (BC), on the contrary, presents the advantages of simple and reliable structure. It uses gas as working fluid which does not involve phase change during the expansion [22]. Thus, Brayton-ORC systems can be used to exploit the waste heat from ICE effectively and safely.

Quite a few studies have been published to improve the waste heat recovery from exhaust gas. Jacket water, though explored by some researchers, is mainly used as the low-temperature heat source to preheat the organic working fluid in ORC. However, the mismatching mass flow rate of organic working fluid in the preheater and the evaporator causes a large amount of heat waste in jacket water. Yu et al. [23] calculated the energy recovery efficiency from an ORC- based ICE waste heat recovery system. 75% waste heat could be recovered from exhaust gas while 9.5% waste heat was recovered from jacket water. But for most ICEs (rated power between 500 kW and 2000 kW), discharged thermal energy in jacket water is approximately the same as the energy in exhaust gas [24]. Thus, a large amount of waste heat in jacket water is potentially valuable for recovery.

Usually, traditional power plants only generate power and can't fulfill the requirements of the consumers for energy supply. Cooling capacity, for example, is needed in many places such as hospital, hotel, restaurant, etc. To satisfy the various demands of the consumers and to recover the waste heat more efficiently, cogeneration systems is introduced by many researchers. Cogeneration systems driven by waste heat in internal combustion engines were developed by a number of investigators. Chen et al. [25] designed an ammonia-water combined cooling and power system using the waste heat from the ICEs. Ammonia-water was heated by exhaust gas and jacket water. One part of the ammonia-water vapor flew into the turbine to provide power and the other part flew into the evaporator to provide refrigeration. Salek et al. [26] coupled an ammonia absorption refrigeration cycle and a bottoming Rankine cycle with internal combustion engine to produce power and cooling capacity. Absorption refrigeration cycles were considered by most of the combined cooling and power systems to convert exhaust gas waste heat to cooling capacity. However, ejector refrigeration cycle, which presents the advantages of desirable efficiency, small structure and simple layout [27,28], is always neglected.

In this study, a combined cooling and power system is developed, which comprises a CO2 Brayton cycle, a dual-pressure ORC and an ejector refrigeration cycle. The CO2 Brayton cycle is used to recover the waste heat from high-temperature exhaust gas directly. The turbine exhaust in the CO2 Brayton cycle and the engine exhaust gas after heat transfer are respectively regarded as the heat sources for the high-pressure side and low-pressure side of the dual-pressure ORC, realizing the cascading utilization of exhaust gas waste heat. Meanwhile, organic working fluid in high-pressure side and low-pressure side are both preheated by jacket water to make full use of the waste heat. What's more, the ejector refrigeration cycle is adapted to recover the waste heat of jacket water further and produce cooling capacity simultaneously. Thermodynamic and exergoeconomic analysis is carried out to examine the effects of key parameters on system performances. Then a system optimization is conducted to obtain the minimum levelized exergy cost for the system product by means of genetic algorithm.

2. System description

2.1. CCP system

The combined cooling and power (CCP) system is shown in Fig 1. The system integrates a dual-pressure organic Rankine cycle with a CO_2 Brayton cycle and an ejector refrigeration, which can produce power and cooling capacity simultaneously. The exhaust gas from the internal consumption engine enters the gas heater to drive the CO_2 Brayton cycle. CO_2 cooled by the precooler flows through the compressor to be compressed to a supercritical state. Then the high-pressure CO_2 absorbs heat in the gas heater, becoming high-pressure and high-temperature state, and enters BC turbine to produce power.

After expanding in the BC turbine, the high-temperature exhaust CO_2 flows into vapor generator 2 to heat the organic working fluid. High-pressure side organic working fluid heated by the CO_2 then flows into the ORC turbine to produce power. Meanwhile low-pressure side organic working fluid absorbs heat from the secondary engine exhaust gas in vapor generator 1 and then enters ORC turbine to produce power.

Exhaust vapor from the ORC turbine is cooled by condenser 1 to liquid state and pressured by pump 1. Jacket water with large mass flow rate is used to preheat the organic working fluid in the preheater. The preheated organic working fluid then separates. One part of the fluid is pumped by pump 3 to the vapor generator 1 to cycle in the low-pressure side. The other part is pumped by pump 2 to the vapor generator 2 to cycle in the high-pressure side.

The jacket water then flows into vapor generator 3 to provide heat for the ejector refrigeration cycle. After the condensation process in condenser 2, liquid working fluid is divided into two separated parts. One part of the fluid is pumped to the vapor generator 3 to absorb heat from jacket water and then becomes superheated vapor. The other part of the working fluid flows through the throttle valve to become low-pressure vapor-liquid mixture. The low-pressure mixture enters the evaporator to produce cooling capacity when absorbing heat from the environment and become low-pressure vapor. After that, the superheated vapor mixes with the low-pressure vapor in the ejector. The mixed working fluid enters the condenser 2 to be condensed to liquid.

R245fa is selected as the working fluid for the organic Rankine cycle and the ejector refrigeration cycle because of the great thermodynamic performance and the low environment effect [29,30].

3. System model

Several assumptions are made to simplify the simulation of the system.

(1) The system keeps a steady state.

(2) The heat and friction losses in the system are not considered.

(3) The pressure losses in the vapor generator, preheater, precooler, evaporator and condenser are neglected.

(4) Considering the low gas acid dew point temperature, the gas temperature at the outlet of the vapor generator 1 is higher than 110℃[31].

(5) The working fluid out of the condensers and preheater is saturated liquid and the state at the outlet of the evaporator is saturated vapor.

(6) The process through the throttle valve is isenthalpic.

3.1. Thermodynamic model

3.1.1. Energy model

The net power of the CO_2 Brayton cycle is expressed as:

$$W_{\mathrm{BC}} = W_{\mathrm{Bt}} - W_{\mathrm{comp}} \tag{1}$$

The net power of the DORC is given as:

$$W_{\mathrm{ORC}} = W_{\mathrm{Ot}} - W_{\mathrm{p1}} - W_{\mathrm{p2}} - W_{\mathrm{p3}} \tag{2}$$

The cooling capacity of the ERC is given as:

$$Q_{\mathrm{cool}} = M_{\mathrm{cool}} \cdot (h_{21} - h_{20}) \tag{3}$$

The net power output of the whole system is calculated as:

$$W_{\mathrm{net}} = W_{\mathrm{ORC}} + W_{\mathrm{BC}} - W_{\mathrm{p4}} \tag{4}$$

The thermal efficiency of the system is given as:

$$\eta_{\mathrm{th}} = \frac{W_{\mathrm{net}} + Q_{\mathrm{cool}}}{M_{\mathrm{g1}} \cdot (h_{\mathrm{g1}} - h_{\mathrm{g3}}) + M_{\mathrm{w1}} \cdot (h_{\mathrm{w1}} - h_{\mathrm{w3}})} \tag{5}$$

The detailed energy model equations of each component are list in Table 1. Note that there are two expanding processes in the ORC turbine. The high-pressure side vapor expands from high pressure (state 10) to low pressure (state 11) for the first time and then mixes with the low-pressure side vapor. After that, the mixed vapor expands from low pressure (state 11) to the back pressure of ORC turbine (state 12) for the secondary time.

3.1.2. Exergy model

In general, the energy model of a system is based on the first law of the thermodynamic which focuses the amount of the thermal energy in the system. The exergy model of the system is based on the second law of the thermodynamic which focuses on the quality of the thermal energy. The exergy analysis of the system is based on a dead state (the ambient conditions in this paper). The equation of exergy for unit working fluid is expressed as:

$$e = (h - h_0) - T_0 \cdot (s - s_0) \quad (6)$$

where h_0, T_0 and s_0 are the parameters under the ambient conditions.

The exergy flow rate in this study is given by:

$$E = M \cdot e \quad (7)$$

All the components in the system are associated directly or indirectly with fuel or other heat sources, such as exhaust gas and jacket water in this study. The heat sources provide exergy for the components to operate. For each component, there is an exergy balance equation, being expressed as [32]:

$$E_{\mathrm{F}} = E_{\mathrm{P}} + E_{\mathrm{D}} + E_{\mathrm{L}} \quad (8)$$

where E_{F} is the rate of exergy for the component fuel and E_{P} represents the rate of exergy for the component product; E_{D} denotes the rate of component exergy destruction and E_{L} expresses the rate of exergy loss for the component.

The details of the exergy balance equations for each component are listed in Table 1.

The exergy efficiency represents the degree of the utilization of the waste heat in the system, being expressed as:

$$\eta_{\mathrm{ex}} = \frac{W_{\mathrm{net}} + E_{\mathrm{cool}}}{E_{\mathrm{g1}} - E_{\mathrm{g3}} + E_{\mathrm{w1}} - E_{\mathrm{w3}}} \quad (9)$$

where E_{cool} is the exergy rate of the cooling process, being expressed as:

$$E_{\mathrm{cool}} = E_{25} - E_{24} \quad (10)$$

3.2. Capital cost and exergoeconomic model of the system

3.2.1. Capital cost calculation

In this study, a method of modeling the capital costs of the main component is employed [33]. At first, the bare module cost of the components is calculated as the basic cost. The basic cost of the components includes the direct project cost (such as equipment cost, material cost for the installation, etc.) and the indirect project cost (like the taxes, insurance engineering expenses etc.). The bare module cost of the components is calculated under basic conditions. For conditions different from the basic conditions, multiplying factors (the specific equipment type, the specific system pressure and the specific material of construction) are added in the calculation to correct the results.

Axial turbines (BC turbine and ORC turbine) are used in this study. The bare module cost equation of the turbine is:

$$\log_{10} C_{\mathrm{turb}}^{0} = K_{1,\mathrm{turb}} + K_{2,\mathrm{turb}} \cdot \log_{10} W + K_{3,\mathrm{turb}} \cdot (\log_{10} W)^2 \tag{11}$$

where K_{turb} is constant corresponding to the turbine type; W is the power output of the turbine.

Turbines used in this study are made of carbon steel (CS) and operate under high pressure. Thus, a multiplying factor is used to correct the result. The capital cost of the turbine is given as:

$$C_{\mathrm{turb}} = F_{\mathrm{BM,turb}} \cdot C_{\mathrm{turb}}^{0} \tag{12}$$

where $F_{\mathrm{BM,turb}}$ is the multiplying factor corresponding to the working conditions of the turbine.

Reciprocating pumps are used in this study. The bare module cost equation of the pumps is given as:

$$\log_{10} C^0_{\text{pump}} = K_{1,\text{pump}} + K_{2,\text{pump}} \cdot \log_{10} W + K_{3,\text{pump}} \cdot (\log_{10} W)^2 \tag{13}$$

where K_{pump} is constant corresponding to the pump type; W is the power input of the pump.

Pumps used in this study are made of stainless steel (SS) and work under high pressure. Thus, multiplying factors are used to correct the bare module cost. The capital cost of the pump is given as:

$$C_{\text{pump}} = \left(B_{1,\text{pump}} + B_{2,\text{pump}} \cdot F_{\text{M,pump}} \cdot F_{\text{P,pump}}\right) \cdot C^0_{\text{pump}} \tag{14}$$

where B_{pump} is constant corresponding to the type of the pump; $F_{\text{M,pump}}$ is the material factor of the pump and $F_{\text{P,pump}}$ is the pressure factor of the pump. The equation of the pressure factor is given as:

$$\log_{10} F_{\text{P,pump}} = C_{1,\text{pump}} + C_{2,\text{pump}} \cdot \log_{10} P_{\text{pump}} + C_{3,\text{pump}} \cdot (\log_{10} P_{\text{pump}})^2 \tag{15}$$

where C_{pump} is the constant corresponding to the type of the pump and P_{pump} is the pressure of the pump under working conditions.

Axial compressor is used in this study. The bare module cost equation of the compressor is given as:

$$\log_{10} C^0_{\text{comp}} = K_{1,\text{comp}} + K_{2,\text{comp}} \cdot \log_{10} W + K_{3,\text{comp}} \cdot (\log_{10} W)^2 \tag{16}$$

where K_{comp} is the constant corresponding to the type of the compressor; W is the power input of the compressor.

The compressor is made of carbon steel (CS) and works under high pressure.

Correction equation of the bare module cost is given as:

$$C_{\mathrm{comp}} = F_{\mathrm{BM,comp}} \cdot C_{\mathrm{comp}}^{0} \tag{17}$$

where $F_{\mathrm{BM,comp}}$ is the constant corresponding to the type of the compressor.

Tube-and-shell heat exchangers (gas heater, vapor generators, precooler, preheater, evaporator and condensers) are used in this study. The bare module cost equation of the heat exchanger is given as:

$$\log_{10} C_{\mathrm{he}}^{0} = K_{1,\mathrm{he}} + K_{2,\mathrm{he}} \cdot \log_{10} A + K_{3,\mathrm{he}} \cdot (\log_{10} A)^{2} \tag{18}$$

where K_{he} is the constant corresponding to the type of the heat exchanger; A is the heat transfer area of the heat exchanger. The calculation of the heat exchanger areas is presented in Appendix A.

Heat exchangers used in this study are made of carbon steel (CS) and work under different pressure. Multiplying factors are needed to correct the results, the equation is given as:

$$C_{\mathrm{he}} = \left(B_{1,\mathrm{he}} + B_{2,\mathrm{he}} \cdot F_{\mathrm{M,he}} \cdot F_{\mathrm{P,he}}\right) \cdot C_{\mathrm{he}}^{0} \tag{19}$$

where B_{he} are the constants correspond to the type of the heat exchanger. $F_{\mathrm{M,he}}$ and $F_{\mathrm{P,he}}$ are the material factor and pressure factor, respectively. The pressure factor is obtained from the following equation:

$$\log_{10} F_{\mathrm{P,he}} = C_{1,\mathrm{he}} + C_{2,\mathrm{he}} \cdot \log_{10} P_{\mathrm{he}} + C_{3,\mathrm{he}} \cdot (\log_{10} P_{\mathrm{he}})^{2} \tag{20}$$

where C_{he} is the constant corresponding to the type of the heat exchanger; P_{he} is the designed working pressure for the heat exchanger.

The values of the constants mentioned above for the main components are listed in Appendix B.

The calculation of the bare module cost depends on past records or published correlations for price information. It is necessary to update the costs because of the changing economic conditions (inflation). This can be achieved by the following expression:

$$C_2 = C_1 \cdot \left(\frac{I_2}{I_1} \right) \tag{21}$$

where C is the purchased cost and I is the cost index. The subscript 1 refers to base time when cost is known and subscript 2 refers to time when cost is desired. The *CEPCI* (Chemical Engineering Plant Cost Index) is employed to calculate the inflation. The values of $CEPCI_{2016}$ and $CEPCI_{\mathrm{ref,2001}}$ are 541.7 and 397, respectively [34,35].

3.2.2. Exergoeconomic model

Exergoeconomic is a branch of engineering which combines the thermodynamic analysis and economic principles. Thermodynamic performance and economic cost of the system are all taken into consideration.

To find the relationship between the present value of the expenditure and the equivalent annually levelized costs, the capital recovery factor (CRF) is employed, being expressed as [32]:

$$Z_{\mathrm{i}} = CRF \cdot C_{\mathrm{i}} \tag{22}$$

$$CRF = \frac{i_{\mathrm{eff}} \cdot \left(1 + i_{\mathrm{eff}}\right)^n}{(1 + i_{\mathrm{eff}})^n - 1} \tag{23}$$

where i_{eff} is the effective discount rate with a value of 0.05 [36]; n is the lifetime of the CCP system being assumed as 30 [37].

In order to calculate the equivalent annually levelized costs, the annual working time of the system is assumed as 8000 h [38]. Then the annual exergy rates and annual power output or consumption are obtained.

In a steady system, there are a number of entering and outing working fluid steams and heat and work interactions with the surroundings. In exergoeconomic analysis, each flowing steam is associated with a levelized exergy cost. The equations to calculate the cost of the steam product are given as:

$$C_{\mathrm{in}} = c_{\mathrm{in}} \cdot E_{\mathrm{y,in}} \tag{24}$$

$$C_{\mathrm{out}} = c_{\mathrm{out}} \cdot E_{\mathrm{y,out}} \tag{25}$$

$$C_{\mathrm{work}} = c_{\mathrm{work}} \cdot W_{\mathrm{y}} \tag{26}$$

$$C_{\mathrm{heat}} = c_{\mathrm{heat}} \cdot E_{\mathrm{y,heat}} \tag{27}$$

where c denotes levelized exergy cost of the steams; $E_{\mathrm{y,in}}$ and $E_{\mathrm{y,out}}$ are the exergy transfer rate of the steam flowing in and out a component; W_{y} and $E_{\mathrm{y,heat}}$ are the power and the heat transfer rate of the components considering the annual working time.

The cost balance equation applied to the kth system component is given as:

$$\sum\nolimits_{\mathrm{out}} C_{\mathrm{out,k}} + C_{\mathrm{w,k}} = C_{\mathrm{heat,k}} + \sum\nolimits_{\mathrm{in}} C_{\mathrm{in,k}} + Z_{\mathrm{k}} \tag{28}$$

Details of the cost balance equation are listed in Table 2.

The levelized exergy cost for system product is chosen to indicate the exergoeconomic performance, being expressed as [39,40]:

$$c_{\mathrm{product}} = c_{\mathrm{capital}} + c_{\mathrm{fuel}} \tag{29}$$

where c_{capital} is the capital-cost-related part of the levelized exergy cost for the system product, being expressed as:

$$c_{\text{capital}} = \frac{Z_{\text{total}}}{W_{\text{net}} + E_{\text{cool}}} \tag{30}$$

c_{fuel} is the fuel-cost-related part of the levelized exergy cost for the system product, being expressed as:

$$c_{\text{fuel}} = \frac{c_{\text{Bt}} \cdot W_{\text{y,comp}} + c_{\text{Ot}} \cdot W_{\text{y,pump1}} + c_{\text{Ot}} \cdot W_{\text{y,pump2}} + c_{\text{Ot}} \cdot W_{\text{y,pump3}} + c_{\text{Ot}} \cdot W_{\text{y,pump4}}}{W_{\text{net}} + E_{\text{cool}}} \tag{31}$$

c_{Bt} and c_{Ot} are the levelized exergy cost for the BC turbine power output and the ORC turbine power output, which are calculated in Table 3. Likewise, they can be expressed as the capital-cost-related part and the fuel-cost-related part:

$$c_{\text{Bt}} = \frac{Z_{\text{Bt}}}{W_{\text{y,Bt}}} + \frac{c_3 \cdot \left(E_{\text{y,3}} - E_{\text{y,4}}\right)}{W_{\text{y,Bt}}} \tag{32}$$

$$c_{\text{Ot}} = \frac{Z_{\text{Ot}}}{W_{\text{y,Ot}}} + \frac{c_{10} \cdot \left(E_{\text{y,10}} + E_{\text{y,11}} - E_{\text{y,12}}\right)}{W_{\text{y,Ot}}} \tag{33}$$

In addition, the levelized exergy cost for the condensers and the precooler is equal to zero, being given by:

$$c_{26}=c_{28}=c_{30}=0 \tag{34}$$

The levelized exergy cost for the exhaust gas as well as the jacket water is zero, being expressed as:

$$c_{\text{g1}}=c_{\text{w1}}=0 \tag{35}$$

4. Results and discussion

4.1.1. Simulation conditions for the system

The thermodynamic parameters of the working fluid are calculated under the environment of MATLAB with the help of REFPROP 9.1 [41]. The basic conditions of simulation for the CCP system are listed in Table 3

4.1.2. Internal combustion engine

In this study, the engine selected [8] is a 12-cylinder 4-stroke supercharged gas engine. The main designed parameters of the engine are listed in Table 4. The composition of the engine exhaust gas is presented in Table 5. The heat load capacity of the engine exhaust gas is about 1700 kW when cooled down to the acid dew temperature and the 1000 kW can be obtained from the engine jacket water.

4.2. Analysis for the thermodynamic and exergoeconimic performance

Seven key parameters (BC turbine inlet temperature, BC turbine inlet pressure, inlet temperature at the high-pressure side of ORC turbine, inlet pressure at the high-pressure side of ORC turbine, inlet temperature at the low-pressure side of ORC turbine, inlet pressure at the low-pressure side of ORC turbine and the ejector primary inlet pressure) are chosen to analyze the thermodynamic and exergoeconomic performance of the system. In the thermodynamic aspect, the net power output of the CO_2 Brayton cycle (W_{BC}), net power output of the DORC (W_{ORC}), net power of the whole system (W_{net}), cooling capacity of the system (Q_{cool}) and the exergy efficiency of the system (η_{exergy}) are selected to reflect the system performance. Levelized exergy cost for the BC turbine power output (c_{Bt}), levelized exergy cost for the ORC turbine power output (c_{Ot}), levelized exergy cost the system product ($c_{product}$) and the system capital cost ($z_{capital}$) are chosen to represent the exergoeconomic performance.

4.2.1. Variations of thermal parameters in CBC

The influences of the BC turbine inlet temperature on the output and the exergy efficiency of the system are shown in Fig. 2. The net power output of the CO_2 Brayton cycle (CBC) increases with the rise of the BC turbine inlet temperature. That can be explained by the decrease of the compressor power consumption. With the increase of the CO_2 temperature at the BC turbine inlet, the mass flow rate of CO_2 decreases. As a result, less CO_2 working fluid is compressed by the compressor, leading to the decrease of the compressor power consumption. On the one hand, the decrease of the mass flow rate cuts down the BC turbine power output. On the other hand, the increase of inlet temperature causes the increase of enthalpy drop of CO_2 in the turbine which results in the increase of the BC turbine power output. The two effects mention above cause the slight decrease of the BC turbine power output, which is smaller than the decrease of the compressor power consumption. Thus, the large decrease of the compressor power consumption determines the increase of the CBC net power output.

It is presented that the net power output of the DORC increases with the rise of the BC turbine inlet temperature. The temperature of the exhaust CO_2 increases with the increase of BC turbine inlet temperature. Since the exhaust CO_2 acts as the heat source for organic working fluid in the high-pressure side of DORC, more heat is provided in vapor generator 2. As a result, the mass flow rate of the organic working fluid increases, leading to the rise of the power output of the ORC turbine. The increase of the power consumption of the pumps in the DORC is much smaller than the increase of the ORC turbine power output. Thus, the net power output of the DORC increases.

The net power of the whole CCP system increases with the increase of the BC turbine inlet temperature. That can be explained by the increase of the CO_2 Brayton cycle net power output and the DORC net power output. The increase of the net power output of the system causes the increase of the exergy efficiency of the system.

With the increase of the BC turbine inlet temperature, the cooling capacity of the ejector refrigeration cycle (ERC) decreases, as shown in Fig. 2. As discussed above, the increase of the exhaust CO_2 temperature causes the increase of the organic working fluid mass flow rate in DORC. Thus, more heat is absorbed by the organic working fluid in the preheater from the jacket water. Less heat is available for the ERC working fluid in vapor generator 3. As a result, the mass flow rate of the working fluid in the evaporator decreases, resulting in the decrease of the cooling capacity of the CCP system.

The influences of the BC turbine inlet temperature on the levelized exergy cost and the system capital cost of the system are shown in Fig. 3. The levelized exergy cost for the BC turbine power output decreases with the increase of the BC turbine inlet temperature. Since the decrease of the compressor power consumption, the cost of compressor decreases. According to Eq. (32), the decrease of compressor cost leads to the decrease of capital-cost-part of the levelized exergy cost for the BC turbine power output c_{Bt}. Thus, c_{Bt} decreases. The levelized exergy cost for the ORC turbine decreases with the increase of the BC turbine inlet temperature. The reason for this is the large increase of the power output of the ORC turbine. The increase of the ORC turbine power output causes the increase of both the capital-cost-related part and fuel-cost-related part of c_{Ot}.

The system capital cost increases with the increase of the BC turbine inlet temperature. Since the large increase of the ORC turbine power output, the cost of the ORC turbine increases. Meanwhile, the increase of the mass flow rate of the organic working fluid in the DORC causes the increase of the cost for the vapor generator 2 and preheater. Though the cost of the compressor decreases with the decrease of the compressor power consumption, the effect of the ORC turbine cost is more important, which determines the rise of the system capital cost.

It can be obtained in Fig. 3 that the levelized exergy cost for the system product decreases with the increase of the BC turbine inlet temperature. As mentioned above, the levelized exergy cost for the BC turbine and ORC turbine decrease. Analyzing from Eq. (31), the fuel-cost-related part of the levelized exergy cost for system product decreases. According to Eq. (30), the increase of system net power output causes the decrease of the capital-cost-related part of the levelized exergy cost for the system product. As a result, the levelized exergy cost for the system product decreases.

The influences of the BC turbine inlet pressure on the output and the exergy efficiency of the system are shown in Fig. 4. The net power output of the CBC increases with the increase of the BC turbine inlet pressure. Since the increase of pressure at BC turbine inlet, the enthalpy drop of the CO_2 in the BC turbine increases, causing the increase of the BC turbine power output. The pressure rise also causes the increase of compressor power consumption. But the increase of the BC turbine power output is larger than the increase of the compressor power consumption. As a result, the net power output of the CBC increases.

The net power output of the DORC decreases with the increase of the BC turbine inlet pressure. On the one hand, the temperature of the exhaust CO_2 at the BC turbine outlet decreases with the increase of the BC turbine inlet pressure. Thus, less heat is provided in vapor generator 2, causing the decrease of the mass flow rate of the organic working fluid in the high-pressure side DORC. As a result, the power output of the high-pressure side DORC decreases. On the other hand, the increase of the BC turbine inlet pressure causes the increase of the compressor power consumption which results in the rise of the CO_2 temperature at the compressor outlet. Thus, less heat is absorbed by CO_2 in the gas heater and more heat is transferred to the organic working fluid in vapor generator 1. The mass flow rate of the organic working fluid in the low-pressure side DORC increases, causing the increase of the power output in the low-pressure side. The increase of the power output in low-pressure side is smaller than the decrease of power output in the high-pressure side. Thus, the net power of the whole DORC decreases.

The cooling capacity of the system increases with the increase of the BC turbine inlet pressure. The decrease of the mass flow rate in the high-pressure side of DORC is more than the increase of the mass flow rate in the low-pressure side. As a result, the total mass flow in the DORC decreases. Thus, less heat is absorbed from the jacket water in the preheater and more heat is available in vapor generator 3 for working fluid in the ERC. The mass flow rate of the working fluid in ERC increases, causing the increase of the cooling capacity.

The net power output of the whole system increases with the increase of the BC turbine inlet pressure. Though the net power output of the DORC decreases, the increase of CBC net power output is much larger than the decrease. As a result, the net power output of the whole system increases. The increase of the net power output of the CCP system causes the increase of the exergy efficiency of the system, as shown in Fig. 4.

The influences of the BC turbine inlet pressure on the levelized exergy cost and the system capital cost of the system are presented in Fig. 5. The levelized exergy cost for the BC turbine output c_{Bt} increases with the increase of the BC turbine inlet pressure. With the increase of the BC turbine output, the cost of the turbine increases, causing the increase of the capital-cost-related part of c_{Bt}. Meanwhile, the increase of the compressor power consumption causes the increase of the levelized exergy cost for the CO_2 at the turbine inlet, resulting in the increase of the fuel-cost-related part of c_{Bt}. As a result, c_{Bt} increases.

The levelized exergy cost for the ORC turbine product c_{Ot} increases with the increase of the BC turbine inlet pressure. The decrease of the mass flow rate in the DORC causes that less exergy is produced by the vapor generator 2. As a result, the levelized exergy cost for the vapor at the high-pressure side of ORC turbine inlet increases, which determines the increase of the fuel-cost-related part of the levelized exergy for the ORC turbine power output. Thus, the levelized exergy cost for the ORC turbine increases.

The system capital cost of increases with the increase of the BC turbine inlet pressure. The increase of the BC turbine power output and the compressor power consumption results in the increase of the BC turbine cost and compressor cost. The increase of the mass flow rate in the ERC causes the increase of capital cost for the evaporator and vapor generator 3. All the cost increase mention above accounts for the increase of the system capital cost.

The levelized exergy cost for the system product decreases with the increase of BC turbine inlet pressure as shown in Fig. 5. According to Eq. (31), the increase of c_{Ot}, c_{Bt} and compressor power consumption could cause the increase of the fuel-cost-related part of the levelized exergy cost for the system product. However, because of the large increase of the system net power output, the capital-cost-related part and the fuel-cost-related part decrease actually. Thus, the levelized exergy cost for the system product decreases.

4.2.2. Variations of thermal parameters in DORC.

The influences of inlet temperature at the high-pressure side of ORC turbine on the output and the exergy efficiency of the system are shown in Fig. 6. The net power output of the CBC remains unchanged. The reason is that the change of thermal parameters in dual-pressure ORC can’t affect the thermodynamic performance of the CBC.

The net power output of the DORC cycle decreases with the increase of inlet temperature at the high-pressure side of ORC turbine. With the increase of the vapor temperature at the high-pressure ORC inlet, the mass flow rate of the organic working fluid in the high-pressure side of DORC decreases. The decrease of organic working fluid mass flow rate causes the decrease of the power output of the ORC turbine, which further causes the decrease of the net power output of the DORC.

The cooling capacity of the ejector refrigeration cycle increases with the rise of inlet temperature at the high-pressure side of ORC turbine. The decrease of the organic working fluid mass flow rate in the DORC results in the decrease of the heat transfer rate in the preheater. More heat is released in vapor generator 3 from the jacket water to the working fluid in the ejector refrigeration cycle, leading to the increase of the working fluid mass flow rate. Consequently, the cooling capacity of the ejector refrigeration cycle increases.

The net power output of the CCP system decreases with the increase of inlet temperature at the high-pressure side of ORC turbine. The increase of the working fluid mass flow rate in the ERC causes the increase of the power consumption of pump 4. Power output of the CBC keeps unchanged and dual-pressure ORC power output decreases. According to Eq. (4), the net power output of the CCP system decreases. The decrease of the CCP system net power output causes the decrease of the exergy efficiency of the system, as shown in Fig. 6.

The influences of inlet temperature at the high-pressure side of ORC turbine on the levelized exergy cost and the system capital cost of the system are presented in Fig. 7. The levelized exergy cost for the ORC turbine (c_{Ot}) increases with the increase of inlet temperature at the high-pressure side of ORC turbine. The can be explained by the decrease of the decrease of the ORC turbine power output.

The levelized exergy cost for the BC turbine power output (c_{Bt}) increases with the increase of inlet temperature at the high-pressure side of ORC turbine. Since the decrease of the mass flow rate in the high-pressure side of ORC, the exergy of the organic working fluid vapor generated by the vapor generator 2 decreases, causing the increase of the levelized exergy cost of the vapor. The organic working fluid vapor is heat by the BC turbine exhaust CO_2. Thus, the increase of the vapor levelized exergy cost causes the increase of the levelized exergy cost for the exhaust CO_2. According to Eq. (32), the increase of the levelized exergy cost for the exhaust CO_2 causes the increase of the fuel-cost-related part of BC turbine levelized exergy cost. As a result, the levelized exergy cost for the BC turbine power output increases.

The system capital cost decreases with the increase of inlet temperature at the high-pressure side of ORC turbine. Because of the decrease of the organic working fluid mass flow rate in the dual-pressure ORC, the cost of the ORC turbine and vapor generator 2 decreases. Thus, the system capital cost decreases.

The levelized exergy cost for the system product ($c_{product}$) increases with the increase of inlet temperature at the high-pressure side of ORC turbine, as shown in Fig. 7. Since the increase of the levelized exergy cost for the BC turbine and ORC turbine power output, the fuel-cost-related part of $c_{product}$ increases. Meanwhile, the large decrease of the net power of the CCP system causes the increase of the capital-cost-related part of $c_{product}$, according to Eq. (30). Thus, levelized exergy cost for the system product increases.

The influences of inlet pressure at the high-pressure side of ORC turbine on the output and the exergy efficiency of the system are presented in Fig. 8. The net power output of the CBC keeps unchanged because of the unchanged thermal parameters in the cycle.

The net power output of the DORC increase with the increase of inlet pressure at the high-pressure side of ORC turbine. The increase of the evaporation pressure cuts down the latent heat of the organic working fluid, which causes the increase of the mass flow rate in the high-pressure side of the DORC. As a result, the net power output of the ORC turbine increases, leading to the increase of the net power output of the DORC.

Considering the increase of the DORC net power output and the unchanged CBC net power output, the net power output of the whole system increases. Also, the exergy efficiency of the system increases.

The increase of the mass flow rate in the DORC absorbs more heat from the jacket water in the preheater. Thus, less heat is released in the vapor generator 3, causing the decrease of the mass flow rate of the working fluid in the ERC. As a result, the cooling capacity of the system decreases.

The influences of inlet pressure at the high-pressure side of ORC turbine on the levelized exergy cost and system capital cost of the system are presented in Fig. 9. The large increase of the net power output accounts for the decrease of the levelized exergy cost for the ORC turbine power output. The increase of the mass flow rate of the organic working fluid in the high-pressure side of the DORC means that more exergy in the vapor is generated by the vapor generator 2. The levelized exergy cost for the vapor at the vapor generator 2 outlet decreases. The exhaust CO_2 of the BC turbine provides heat for the vapor. The decrease of the vapor levelized exergy cost causes the decrease of the exhaust CO_2 levelized exergy cost. Meanwhile, the decrease of the levelized exergy cost for the CO_2 causes results in the decrease of the fuel-cost-related part of the levelized exergy cost for the BC turbine output. As a result, the levelized exergy cost for the BC turbine power output decreases.

The increase of the ORC turbine power output and the increase of mass flow rate in the DORC cause the increase of the turbine cost and the vapor generator 2 cost, respectively. Thus, the system capital cost increases.

The levelized exergy cost for the system product decreases with the increase of inlet pressure at the high-pressure side of ORC turbine. The decrease of the levelized exergy cost for the ORC turbine power output and the BC turbine power output accounts the decrease of the fuel-cost-related part of the levelized exergy cost for the system product. The increase of the system net power outweighs the increase of the system capital cost. Thus, the capital-cost-related part of the levelized exergy cost of the system product. As a result, the levelized exergy cost of the system product decreases.

The influences of inlet temperature at the low-pressure side of ORC turbine on the output and the exergy efficiency of the system are presented in Fig. 10. Parameters changes in the DORC can't affect the thermodynamic performance of the CBC. Thus, the net power output of the CBC remains unchanged.

The net power of the DORC decreases with the increase of inlet temperature at the low-pressure side of ORC turbine. The increase of the inlet temperature causes the decrease of the mass flow rate in the low-pressure side of DORC, leading to the decrease of the DORC net power output.

Considering the decrease of the DORC net power output and the unchanged CBC net power output, the net power output of the whole system decreases. Also, the exergy efficiency of the system decreases.

The cooling capacity of the ejector refrigeration cycle increases with the increase of inlet temperature at the low-pressure side of ORC turbine. The increase of the inlet temperature causes the decrease of the mass flow rate of the organic working fluid in the low-pressure cycle. Thus, less heat is absorbed from the jacket water in the preheater and more heat is released in vapor generator 3. The mass flow rate of the working fluid in the ERC increases, leading to the increase of the cooling capacity.

The influences of inlet temperature at the low-pressure side of ORC turbine on the levelized exergy cost and system capital cost of the system are presented in Fig. 11. The levelized exergy cost for the BC turbine power output increases with the increase of inlet temperature at the low-pressure side of ORC turbine. Though the enthalpy of the organic working fluid increases with the increase of the low-pressure side inlet temperature, the decrease of the mass flow rate causes the decrease of the exergy provided by the vapor generator 1. Thus, the levelized exergy cost of the vapor generated by vapor generator 1 increases. The levelized exergy cost for vapor in vapor generator 2 is the equal to the levelized exergy cost for vapor in vapor generator 1. As a result, the levelized exergy cost for the vapor generator 2 vapor increases, causing the increase of the levelized exergy cost of the exhaust CO_2 after the BC turbine. The increase of the levelized exergy cost for the exhaust CO_2 causes the increase of the levelized exergy cost of the BC turbine power output.

The levelized exergy cost for the ORC turbine (c_{Ot}) increases with the increase of inlet temperature at the low-pressure side of ORC turbine. As mentioned above, the levelized exergy cost for the vapor at the low-pressure side of ORC turbine inlet increases. Thus, the fuel-cost-related part of the levelized exergy cost for the ORC turbine output increases. Also, the decrease of the ORC turbine power output causes the increase both the fuel-cost-related part and the capital-cost-related part. As a result, the levelized exergy cost for the ORC turbine power output increases.

The decrease of the mass flow rate and the ORC turbine power output cause the decrease of the vapor generator 1 cost and the turbine cost. Thus, the capital cost of the system decreases.

The levelized exergy cost for the system product increases with the increase of inlet temperature at the low-pressure side of ORC turbine. The increase of c_{Bt} and c_{Ot} cause the increase of the fuel-cost-related part of the levelized exergy cost for the system product. Though, the decrease of the system capital cost causes the decrease of the capital-cost-related part, its effect is less important. Thus, the increase of the fuel-cost-related part determines the increase of the levelized exergy cost for the system product.

The influences of the inlet pressure at the low-pressure side of ORC turbine on the output and the exergy efficiency of the system are shown in Fig. 12. The net power of the CBC keeps unchanged with the increase of the increase of the low evaporation pressure. That reason is that the thermodynamic performance of the CBC is irrelevant to the thermal parameters in DORC.

The net power output of the DORC increases with the increase of inlet pressure at the low-pressure side of ORC turbine. The increase of inlet pressure at the low-pressure side of ORC turbine causes the increase of the enthalpy drop of the organic working fluid in the ORC turbine. Though the mass flow rate of the working fluid decreases as well, the effect of the enthalpy drop is more important. Thus, the net power of the DORC increases.

The unchanged CBC power output and the increase of the DORC power accounts for the increase of the system net power output. The exergy efficiency of the system increases as a result.

The cooling capacity increases with the increase of inlet pressure at the low-pressure side of ORC turbine. Because of the decrease of the mass flow rate in the DORC, less heat is absorbed in the preheater and more heat is provided in vapor generator 3. Thus, the mass flow rate of the working fluid in the ERC increases, causing the increase of the cooling capacity.

The influences of inlet pressure at the low-pressure side of ORC turbine on the levelized exergy cost and system capital cost of the system are shown in Fig. 13. The levelized exergy cost for the ORC turbine power output decreases with the increase of inlet pressure at the low-pressure side of ORC turbine. The reason is that the decrease of the mass flow rate in the DORC cuts down the capital cost of the vapor generator 1. The power output of the DORC increases as well. Thus, both the capital-cost-related part and the fuel-cost-related part of the system decrease. Consequently, the levelized exergy cost of the ORC turbine power output decreases.

The levelized exergy cost for the BC turbine power output decreases with the increase of the inlet pressure at the low-pressure side of ORC turbine. The decrease of the levelized exergy cost causes the decrease of the levelized exergy cost for the vapor at vapor generator 2 inlet. The vapor is heated by the exhaust CO_2 in the CBC. Thus, the decrease of the vapor levelized exergy cost results in the decrease of the CO_2 levelized exergy cost which determines the fuel-cost-related part of the BC turbine power levelized exergy cost. As a result, the levelized exergy cost for the BC turbine power output decreases.

The increase of the ORC turbine power output causes the increase of the ORC turbine cost. Meanwhile, the increase of the cooling capacity causes the increase of the heat transfer area in the evaporator which requires the rise of the evaporator cost. Thus, the capital cost of the system increases.

The levelized exergy cost for the system product decreases with the increase of inlet pressure at the low-pressure side of ORC turbine. The decrease of the levelized exergy cost of the BC turbine power output and ORC turbine power output cause the decrease of the fuel-cost-related part of the system levelized exergy cost, which determines the decrease of the levelized exergy cost for the system product.

4.2.3. Variations of thermal parameters in ERC.

The influences of the ejector primary inlet pressure on the output and the exergy efficiency of the system are shown in Fig. 14. Thermal parameters changes in the ERC can’ affect the thermodynamic performance of the CBC and DORC. Thus, the net power output of the two cycles remain unchanged. With the increase of the ejector primary inlet pressure, the power consumption of pump 4 increases, leading to the slight decrease of the net power output of the whole system.

Since the entrainment ratio of the ejector increases with the increase of the ejector primary inlet pressure. More working fluid in the is entrained to the ejector from the ejector secondary inlet. Thus, the mass flow rate of the working fluid in the evaporator increases, leading to the increase of the cooling capacity.

With the increase of the ejector primary inlet pressure, the power consumption of pump 4 increase gradually. At first, the exergy loss in the pump 4 power consumption is smaller than the exergy produced in the cooling capacity. Then, the power consumption becomes larger. Thus, the exergy efficiency for the system increases at first and then decreases with the increase of the ejector primary inlet pressure.

The influences of the ejector primary inlet pressure on the levelized exergy cost and the system capital cost of the system are presented in Fig. 15. The increase of the ejector primary inlet pressure can't affect the power output of the BC turbine and ORC turbine. Thus, the levelized exergy cost for the BC turbine and ORC turbine output remain unchanged.

The increase of the pump power consumption results in the increase of the pump 4 cost. The increase of the mass flow rate in the evaporator causes the increase of evaporator cost. Thus, the system capital cost increases. The increase of the system capital cost causes the increase of the capital-cost-related part of $c_{product}$. As a result, the levelized exergy cost for the system product increases.

4.3. System optimization

The parametric analysis reveals the potential of optimization for the CCP system. With the increase of the BC turbine inlet temperature, the net power output of the system increases while the cooling capacity decreases. With the increase of the inlet temperature at the high-pressure side of ORC turbine, the net power output of the system decreases while the cooling capacity increases. In this study, seven key parameters (BC turbine inlet temperature, BC turbine inlet pressure, inlet temperature at the high-pressure side of ORC turbine, inlet pressure at the high-pressure side of

ORC turbine, inlet temperature at the low-pressure side of ORC turbine, inlet pressure at the low-pressure side of ORC turbine and the ejector primary inlet pressure) are chosen as the variables to optimize the system. The ranges of these parameters are listed in Table 6.

Considering that the levelized exergy cost reflects the thermodynamic and the exergoeconomic aspect of the system, the levelized exergy cost for the system product is selected as the objective function and genetic algorithm is selected to conduct the single-objective optimization.

Genetic algorithm (GA) is an optimization method based on the natural biological evaluation. [42] It simulates the natural genetic rules and searches the optimization result in all the generation. The control parameters of the GA are listed in Table 7.

The optimization results of GA are listed in Table 8. It can be obtained that the minimum levelized exergy cost for the system product $c_{product}$ is 53.25 \$ (MWh)$^{-1}$. The exergy efficiency of the CCP system is 37.31% which is also desirable.

5. Conclusion

In this paper, a combined cooling and power system is developed. Seven parameters (temperature and pressure at the inlet of BC turbine, temperature at the high-pressure inlet and the low-pressure inlet of the ORC turbine, high-pressure side and low-pressure side evaporation pressure in DORC and the ejector primary inlet pressure) are selected to analyze the thermodynamic and exergoeconomic performance of the system. Single-objective optimization is carried out with the help of GA. The conclusions of this study are presented as follows:

(1) Both the increase of the BC turbine inlet temperature and pressure contribute to the increase of the exergy efficiency and the decrease of the levelized exergy cost for the system product.

(2) For both the high-pressure side and the low-pressure side of the DORC, the increase of the ORC turbine inlet temperature causes the decrease of exergy efficiency and the increase of the levelized exergy cost for the system product while the increase of the ORC turbine inlet pressure results in the increase of exergy efficiency and the decrease of the levelized exergy cost.

(3) The ERC performance analysis shows that the increase of the ejector primary inlet pressure causes the increase of the cooling capacity and the decrease of system net power output. Levelized exergy cost for the system product increases with the increase of ejector primary inlet pressure.

(4) Single-objective optimization results show that the minimum levelized exergy cost for the system product is obtained as 53.25 $\$(MWh)^{-1}$ with net power output of 374.37 kW, cooling capacity of 188.63 kW and system exergy efficiency of 37.31%.

Acknowledgement

The authors gratefully acknowledge the financial support by the National Natural Science Foundation of China (Grant No. 51476121)

Appendix A

This section shows the calculation of the heat transfer area in the heat exchangers used in this study.

All the heat exchangers used in this study are tube-and-shell heat exchanger. The thermodynamic properties of the working fluid vary with the heat transfer process. Thus, to calculate the heat transfer area actually, the heat transfer processes are discretized into a lot of small sections. In each section, the heat transfer area is small and the thermodynamic properties are assumed to be constant.

For each section the heat transfer area is calculated as:

$$A_{\mathrm{i}} = Q_{\mathrm{i}} \Big/ \left(\Delta T_{\mathrm{i}} \cdot U_{\mathrm{i}}\right) \tag{B1}$$

where ΔT_{i} is the log-mean temperature difference (LMTD) and U_{i} is the overall heat transfer coefficient.

$$\frac{1}{U_{\mathrm{i}}} = \frac{1}{\alpha_{\mathrm{t,i}}} + \frac{\delta}{\lambda} + \frac{1}{\alpha_{\mathrm{s,i}}} \tag{B2}$$

In Eq. (B2) δ and λ represent the thickness of the tube and the thermal conductivity of the tube wall, respectively. $\alpha_{\mathrm{t,i}}$ is the convection heat transfer coefficient in the tube side and $\alpha_{\mathrm{s,i}}$ is the convection heat transfer coefficient in the shell side.

For different heat transfer process, the convection heat transfer coefficient has different format. We classify the heat transfer processes into single-phase heat transfer process and two-phase heat transfer process. In gas heater, precooler and the preheater, single-phase heat transfer process happens. In evaporator, two-phase heat transfer process occurs. In vapor generators and the condensers, both the single-phase and the two-phase heat transfer process happen.

In the single-phase heat transfer process, the convection heat transfer coefficient in the tube side and the shell side are expressed as [43]:

$$\alpha_{\mathrm{t,i}} = \frac{\lambda \cdot Nu}{D_{\mathrm{i}}} \tag{B3}$$

$$\alpha_{\mathrm{s,i}} = 0.36\left(\frac{\lambda}{D_{\mathrm{es}}}\right)\cdot\left(\frac{D_{\mathrm{es}}\cdot G_{\mathrm{s}}}{\mu}\right)^{0.55}\cdot \mathrm{Pr}^{\frac{1}{3}}\cdot\left(\frac{\mu}{\mu_{\mathrm{w}}}\right)^{0.14} \tag{B4}$$

In Eq. (B3), the Nusselt number is calculated as [44,45]:

$$Nu = \left[\frac{(f/8)\cdot \mathrm{Re}\cdot \mathrm{Pr}}{12.7(f/8)^{0.5}\cdot\left(\mathrm{Pr}^{2/3}-1\right)+1.07}\right],\ \ for\ \mathrm{Re}<10^4 \tag{B5}$$

$$Nu = \left[\frac{(f/8)\cdot (\mathrm{Re}-1000)\cdot \mathrm{Pr}}{12.7(f/8)^{0.5}\cdot\left(\mathrm{Pr}^{2/3}-1\right)+1.07}\right],\ for\ 10^4<\mathrm{Re}<5\times10^6 \tag{B6}$$

where f is the Darcy frication factor, Re is the Reynolds and Pr is the Prandtl number.

In Eq. (B4), D_{es} is the equivalent diameter of the shell, being expressed as:

$$D_{\mathrm{es}} = \frac{1.10\mathrm{Pt}^2}{D_{\mathrm{out,i}}} - D_{\mathrm{out,i}} \tag{B7}$$

where Pt is the center distance between the tubes.

Evaporation and condensation are two different two-phase heat transfer processes. In this study, the cold organic working fluid flows in the tubes of the heat exchangers. The convection heat transfer coefficient of evaporation and condensation are expressed as [46,47]:

$$\alpha_{\mathrm{ev,i}} = 0.023\left[\frac{G(1-x)}{\mu_1}\right]^{0.8}\cdot \mathrm{Pr}_{\mathrm{l}}^{0.4}\cdot\frac{\lambda_1}{d}\cdot\left[1+3000Bo^{0.86}+1.12\left(\frac{x}{1-x}\right)^{0.75}\cdot\left(\frac{\rho_{\mathrm{l}}}{\rho_{\mathrm{v}}}\right)^{0.41}\right] \tag{B8}$$

$$\alpha_{\mathrm{cond,i}} = 0.023\left[\frac{G(1-x)}{\mu_1}\right]^{0.8}\cdot \mathrm{Pr}_{\mathrm{l}}^{0.4}\cdot\frac{\lambda_1}{d}\cdot\left[(1-x)^{0.8}+\frac{3.8x^{0.76}(1-x)0.04}{P_r^{0.38}}\right] \tag{B9}$$

In Eq. (B9), P_r is the reduced pressure. In Eq. (B8) *B*o is the boiling number, being expressed as:

$$Bo = \frac{q_{\mathrm{m}}}{G \cdot r_{\mathrm{f}}} \tag{B10}$$

Appendix B

The constants for component capital cost calculation are list in Table B1.

Reference

[1] Heywood J. B. Internal combustion engine fundamentals. New York: McGraw-Hill; 1988.

[2] Chao H, Chao L, Hong G, Hui X, You L, Shuang W. The optimal evaporation temperature and working fluids for subcritical Organic Rankine Cycle. Energy 2012; 38: 136-143.

[3] Bombarda P, Invernizzi C, Pietra C. Heat recovery from Diesel engines: A thermodynamic comparison between Kalina and ORC cycles. Applied Thermal Engineering 2010; 30: 212-219.

[4] Kalyan K, Pedro J, Sundar R. Analysis of exhaust waste heat recovery from a dual fuel low temperature combustion engine using an Organic Rankine Cycle. Energy 2010; 35: 2387-2399.

[5] Wei M, Fang J, Ma C, Danish S. Waste heat recovery from heavy-duty diesel engine exhaust gases by medium temperature ORC system. Science China Technological Sciences 2011; 54: 2746-2753.

[6] Srinivasan K, Mago P, Zdaniuk G, Chamra L, Midkiff K. Improving the Efficiency of the Advanced Injection Low Pilot Ignited Natural Gas Engine Using Organic Rankine Cycles. 2008; 130: 022201.

[7] Tian H, Shu G, Wei H, Liang X, Liu L. Fluids and parameters optimization for the organic Rankine cycles (ORCs) used in exhaust heat recovery of Internal Combustion Engine (ICE). Energy 2012; 47: 125-136.

[8] Vaja I, Gambarotta A. Internal Combustion Engine (ICE) bottoming with Organic Rankine Cycles (ORCs). Energy 2010; 35(2): 1084-1093.

[9] Rosset K, Mounier V, Guenat E, Schiffmann J. Multi-objective optimization of turbo-ORC systems for waste heat recovery on passenger car engines. Energy 2018; 159: 751-765.

[10] Zhang H G, Wang E H, Fan B Y. A performance analysis of a novel system of a dual loop bottoming organic Rankine cycle (ORC) with a light-duty diesel engine. Applied Energy 2013;102: 1504-1513.

[11] Yang F, Cho H, Zhang H, Zhang J. Thermoeconomic multi-objective optimization of a dual loop organic Rankine cycle (ORC) for CNG engine waste heat recovery. Applied Energy 2017; 205: 1100-1118.

[12] Ge Z, Li J, Liu Q, Duan Y, Yang Z. Thermodynamic analysis of dual-loop organic Rankine cycle using zeotropic mixtures for internal combustion engine waste heat recovery. Energy Conversion and Management 2018; 166: 201-214.

[13] Chen T, Zhuge W, Zhang Y, Zhang L. A novel cascade organic Rankine cycle (ORC) system for waste heat recovery of truck diesel engines. Energy Conversion and Management 2017;138: 210-223.

[14] Mansoury M, Jafarmadar S, Khalilarya S. Energetic and exergetic assessment of a two-stage Organic Rankine Cycle with reactivity-controlled compression ignition engine as a low temperature heat source. Energy Conversion and Management 2018; 166: 201-214.

[15] Seyedkavoosi S, Javan S, Kota K. Exergy-based optimization of an organic Rankine cycle (ORC) for waste heat recovery from an internal combustion engine (ICE). Applied Thermal Engineering 2017; 126: 447-457.

[16] Rajabloo T, Davide B, Paolo lora. Effect of a partial thermal decomposition of the working fluid on the performances of ORC power plants. Energy 2017; 133:1013-1026.

[17] Shu G, Zhao M, Tian H, Wei H, Liang X, Huo Y, et al. Experimental investigation on thermal OS/ORC (Oil Storage/Organic Rankine Cycle) system for waste heat recovery from diesel engine. Energy 2016; 107: 693-706.

[18] Wang X, Tian H, Shu G. Part-load performance prediction and operation strategy design of organic Rankine cycles with a medium cycle used for recovering waste heat from gaseous fuel engines. Energies 2016; 9: 527.

[19] Miller E, Hendricks T, Peterson R. Modeling Energy Recovery Using Thermo-electric Conversion Integrated with an Organic Rankine Bottoming Cycle. Journal of Electron Mater 2009; 38: 1206-1213.

[20] Miller E, Hendricks T, Wang H, Peterson R. Integrated dual-cycle energy recovery using thermoelectric conversion and an organic Rankine bottoming cycle. Proceedings of the Institution of Mechanical Engineers, Part A: Journal of Power and Energy 2011; 225: 33-43.

[21] Shu G, Wang X, Tian H. Theoretical analysis and comparison of Rankine cycle and different organic Rankine cycles as waste heat recovery system for a large gaseous fuel internal combustion engine. Applied Thermal Engineering 2016; 108: 525-537.

[22] Galindo J, Guardiola C, Dolz V, Kleut P. Further analysis of a compression-expansion machine for a Brayton Waste Heat Recovery cycle on an IC engine. Applied Thermal Engineering 2018; 128: 345-356.

[23] Yu G, Shu G, Tian Hua, Wei H, Liu L. Simulation and thermodynamic analysis of a bottoming Organic Rankine Cycle (ORC) of diesel engine (DE). Energy 2013; 51: 281-290.

[24] Ma J, Liu L, Zhu T, Zhang T. Cascade utilization of exhaust gas and jacket water waste heat from an Internal Combustion Engine by a single loop Organic Rankine Cycle system. Applied Thermal Engineering 2016; 107: 218-226.

[25] Chen Y, Han W, Jin H. Investigation of an ammonia-water combined power and cooling system driven by the jacket water and exhaust gas heat of an internal combustion engine. International Journal of Refrigeration 2017; 82: 174-188.

[26] Salek F, Moghaddam A, Naserian M. Thermodynamic analysis of diesel engine coupled with ORC and absorption refrigeration cycle. Energy Conversion and Management 2017; 140: 240-246.

[27] Wang J, Dai Y, Sun Z, A theoretical study on a novel combined power and ejector refrigeration cycle. International Journal of Refrigeration 2009; 32: 1186-1194.

[28] Ahmadi P, Dincer I, Rosen M. Performance assessment and optimization of a novel integrated multigeneration system for residential buildings. Energy and Buildings 2013; 67: 568-578.

[29] Dai Y, Wang J, Gao L. Parametric optimization and comparative study of organic Rankine cycle (ORC) for low grade waste heat recovery. Energy Conversion Management 2009; 50: 576-582.

[30] Shu G, Zhao M, Tian H, Huo Y, Zhu W. Experimental comparison of R123 and R245fa as working fluids for waste heat recovery from heavy-duty diesel engine. Energy 2016; 115: 756-769.

[31] Zhang J, Zhang H, Yang K, Yang F, Wang Z, Zhao G, et al. Performance analysis of regenerative organic Rankine cycle (RORC) using the pure working fluid and the zeotropic mixture over the whole operating range of a diesel engine. Energy Conversion Management 2014; 84: 282-294.

[32] Adrian Bejan GT, Moran Michael. Thermal design and optimization. New York: Jogn Wiley & Sons; 1996.

[33] Turton R. Analysis, synthesis, and design of chemical processes. 3rd ed. Upper Saddle River, N.J: Prentice Hall; 2009.

[34] Li J, Ge Z, Liu Q, Duan Y, Yang Z. Thermo-economic performance analyses and comparison of two turbine layouts for organic Rankine cycles with dual-pressure evaporation. Energy Conversion and Management, 2018; 164: 603-614.

[35] http://www.chemengonline.com/pci-home

[36] Sheng Z, Huai W, Tao G. Performance comparison and parametric optimization of subcritical organic Rankine cycle (ORC) and transcritical power cycle system for low-temperature geothermal power generation. Applied Energy 2011;88(8):2740-2754.

[37] Tempesti D, Fiaschi D. Thermo-economic assessment of a micro CHP system fueled by geothermal and solar energy. Energy 2013; 58: 45-51.

[38] Velez F, Segovia JJ, Martin MC, Antonlin G, Chejne F, Quijano A. A technical, economical and market review of organic Rankine cycles for the conversion of low-grade heat for power generation. Renewable and Sustainable Energy Reviews, 2012; 16:4175-4189.

[39] Akbari D, Mahmoudi M. Thermoeconomic analysis & optimization of the combined supercritical CO2 (carbon dioxide) recompression Brayton/ organic Rankine cycle. Energy 2014; 78:501-512.

[40] Zare V, Mahmoudi M, Yari M. An exergoeconomic investigation of waste heat recovery from the Gas Turbine-Modular Helium Reactor (GT-MHR) employing an ammonia–water power/cooling cycle. Energy 2013;61. 397-409.

[41] Lemmon EW, Huber ML, McLinden MO. NIST standard reference database 23, reference fluid thermodynamic and transport properties (REFPROP). Version 9.1. National Institute of Standards and Technology; 2010

[42] Wang J, Dai Y, Gao L. Parametric analysis and optimization for a combined power and refrigeration cycle. Applied Energy 2008;85(11):1071-1085

[43] Kern DQ. Process heat transfer. New York: McGraw-Hill; 1950

[44] Kandylas IP, Stamatelos AM. Engine exhaust system design based on heat transfer computation. Energy Conversion Management 1999; 40:1057-1072.

[45] Incropera FP, DeWitt DP. Fundamentals of heat and mass transfer. New York: Wiley; 2002

[46] Gungor KE, Winterton RHS. Simplified general correlation for saturated flow boiling and comparisons of correlations with data. Chemical Engineering Research and Design, 1987; 65:148-156.

[47] Shah MM. A general correlation for heat transfer during film condensation inside pipes. International Journal of Heat and Mass Transfer 1979; 22:547-556.

Figure captions

Fig. 1. Schematic diagram of the CCP system

Fig. 2. Influences of BC turbine inlet temperature on the output and the exergy efficiency of the system.

Fig. 3. Influences of BC turbine inlet temperature on the levelized exergy cost and the system capital cost of the system.

Fig. 4. Influences of BC turbine inlet pressure on the output and the exergy efficiency of the system.

Fig. 5. Influences of BC turbine inlet pressure on the levelized exergy cost and the system capital cost of the system.

Fig. 6. Influences of inlet temperature at the high-pressure side of ORC turbine on the output and the exergy efficiency of the system.

Fig. 7. Influences of inlet temperature at the high-pressure side of ORC turbine on the levelized exergy cost and the system capital cost of the system.

Fig. 8. Influences of inlet pressure at the high-pressure side of ORC turbine on the output and the exergy efficiency of the system.

Fig. 9. Influences of inlet pressure at the high-pressure side of ORC turbine on the levelized exergy cost and the system capital cost of the system.

Fig. 10. Influences of inlet temperature at the low-pressure side of ORC turbine on the output and the exergy efficiency of the system.

Fig. 11. Influences of inlet temperature at the low-pressure side of ORC turbine on the levelized exergy cost and system capital cost of the system.

Fig. 12. Influences of inlet pressure at the low-pressure side of ORC turbine on the output and the exergy efficiency of the system.

Fig. 13. Influences of inlet pressure at the low-pressure side of ORC turbine on the levelized exergy cost and system capital cost of the system.

Fig. 14. Influences of ejector primary inlet pressure on the output and the exergy efficiency of the system.

Fig. 15. Influences of ejector primary inlet pressure on the levelized exergy cost and the system capital cost of the system.

Table 1 Energy and exergy models for each component in CCP system

Component	Energy equation	E_{F}	E_{P}	E_{D}	E_{L}
Gas heater	$M_{\mathrm{g1}} \cdot (h_{\mathrm{g1}} - h_{\mathrm{g2}}) = M_2 \cdot (h_3 - h_2)$	$E_{\mathrm{g1}} - E_{\mathrm{g2}}$	$E_3 - E_2$	$E_{\mathrm{g1}} + E_2 - E_3 - E_{\mathrm{g2}}$	/
BC turbine	$W_{\mathrm{Bt}} = M_3 \cdot (h_3 - h_4) = M_3 \cdot (h_3 - h_{4\mathrm{s}}) \cdot \eta_{\mathrm{Bt}}$	$E_3 - E_4$	W_{Bt}	$E_3 - E_4 - W_{\mathrm{Bt}}$	/
Vapor generator 2	$M_4 \cdot (h_4 - h_5) = M_9 \cdot (h_{10} - h_9)$	$E_4 - E_5$	$E_{10} - E_9$	$E_4 + E_9 - E_5 - E_{10}$	/
Precooler	$M_1 \cdot (h_5 - h_1) = M_{26} \cdot (h_{27} - h_{26})$	/	/	$E_5 + E_{26} - E_1 - E_{27}$	$E_{27} - E_{26}$
Compressor	$W_{\mathrm{comp}} = M_1 \cdot (h_2 - h_1) = M_1 \cdot (h_{2\mathrm{s}} - h_1) / \eta_{\mathrm{comp}}$	W_{comp}	$E_2 - E_1$	$E_1 - E_2 + W_{\mathrm{comp}}$	/
Vapor generator 1	$M_{\mathrm{g2}} \cdot (h_{\mathrm{g2}} - h_{\mathrm{g3}}) = M_8 \cdot (h_{11} - h_8)$	$E_{\mathrm{g2}} - E_{\mathrm{g1}}$	$E_{11} - E_8$	$E_{\mathrm{g2}} + E_8 - E_{11} - E_{\mathrm{g3}}$	/
ORC turbine	$W_{\mathrm{Ot}} = M_{10} \cdot (h_{10} - h_{12}) + M_{11} \cdot (h_{11} - h_{12})$	$E_{10} + E_{11} - E_{12}$	W_{Ot}	$E_{10} + E_{11} - E_{12} + W_{\mathrm{Ot}}$	/
Condenser 1	$M_{12} \cdot (h_{12} - h_{13}) = M_{28} \cdot (h_{29} - h_{28})$	/	/	$E_{12} + E_{28} - E_{13} - E_{29}$	$E_{29} - E_{28}$
Pump 1	$W_{\mathrm{p1}} = M_{13} \cdot (h_{14} - h_{13}) = M_{13} \cdot (h_{14\mathrm{s}} - h_{13}) / \eta_{\mathrm{p1}}$	W_{p1}	$E_{14} - E_{13}$	$E_{13} - E_{14} + W_{\mathrm{p1}}$	/
Preheater	$M_{15} \cdot (h_{15} - h_{14}) = M_{\mathrm{w1}} \cdot (h_{\mathrm{w1}} - h_{\mathrm{w2}})$	$E_{\mathrm{w1}} - E_{\mathrm{w2}}$	$E_{15} - E_{14}$	$E_{\mathrm{w1}} + E_{14} - E_{15} - E_{\mathrm{w2}}$	/
Pump 2	$W_{\mathrm{p2}} = M_7 \cdot (h_9 - h_7) = M_7 \cdot (h_{9\mathrm{s}} - h_7) / \eta_{\mathrm{p2}}$	W_{p2}	$E_9 - E_7$	$E_7 - E_9 + W_{\mathrm{p2}}$	/
Pump 3	$W_{\mathrm{p3}} = M_6 \cdot (h_8 - h_6) = M_6 \cdot (h_{8\mathrm{s}} - h_6) / \eta_{\mathrm{p3}}$	W_{p3}	$E_8 - E_6$	$E_6 - E_8 + W_{\mathrm{p3}}$	/
Vapor generator 3	$M_{23} \cdot (h_{23} - h_{22}) = M_{\mathrm{w2}} \cdot (h_{\mathrm{w2}} - h_{\mathrm{w3}})$	$E_{\mathrm{w2}} - E_{\mathrm{w3}}$	$E_{23} - E_{22}$	$E_{\mathrm{w2}} + E_{22} - E_{23} - E_{\mathrm{w3}}$	/
Condenser 2	$M_{16} \cdot (h_{16} - h_{17}) = M_{30} \cdot (h_{31} - h_{30})$	/	/	$E_{16} + E_{30} - E_{17} - E_{31}$	$E_{31} - E_{30}$
Valve	$h_{19} = h_{20}$	/	/	$E_{19} - E_{20}$	/
Pump 4	$W_{\mathrm{p4}} = M_{22} \cdot (h_{22} - h_{18}) = M_{22} \cdot (h_{22\mathrm{s}} - h_{18}) / \eta_{\mathrm{p4}}$	W_{p4}	$E_{22} - E_{18}$	$E_{18} - E_{22} + W_{\mathrm{p4}}$	/
Ejector	$M_{16} \cdot h_{16} = M_{23} \cdot h_{23} + M_{21} \cdot h_{21}$	$E_{23} + E_{21}$	E_{16}	$E_{23} + E_{21} - E_{16}$	/
Evaporator	$M_{20} \cdot (h_{21} - h_{20}) = M_{24} \cdot (h_{24} - h_{25})$	$E_{20} - E_{21}$	$E_{25} - E_{24}$	$E_{20} + E_{24} - E_{21} - E_{25}$	/

Table 2 Cost balance and auxiliary relation [32] for each component of CCP system

Component	Cost balance	Auxiliary relation

Gas heater	$c_{g2} \cdot E_{y,g2} + c_3 \cdot E_{y,3} = c_{g1} \cdot E_{y,g1} + c_2 \cdot E_{y,2} + Z_{gh}$	$c_{g1}=c_{g2}=0$
Vapor generator 2	$c_5 \cdot E_{y,5} + c_{10} \cdot E_{y,10} = c_4 \cdot E_{y,4} + c_9 \cdot E_{y,9} + Z_{vg,2}$	$c_4=c_5$
BC turbine	$c_4 \cdot E_{y,4} + c_{Bt} \cdot W_{y,Bt} = c_3 \cdot E_{y,3} + Z_{Bt}$	$c_4=c_3$
Precooler	$c_1 \cdot E_{y,1} + c_{26} \cdot E_{y,26} = c_5 \cdot E_{y,5} + c_{27} \cdot E_{y,27} + Z_{prec}$	$c_1=c_5$
Compressor	$c_2 \cdot E_{y,2} = c_1 \cdot E_{y,1} + c_{elec,1} \cdot W_{y,comp} + Z_{comp}$	$c_{elec,1}=c_{Bt}$
Vapor generator 1	$c_{g3} \cdot E_{y,g3} + c_{11} \cdot E_{y,11} = c_{g2} \cdot E_{y,g2} + c_8 \cdot E_{y,8} + Z_{vg,1}$	$c_{g2}=c_{g3}$
ORC turbine	$c_{12} \cdot E_{y,12} + c_{Ot} \cdot W_{y,Ot} = c_{11} \cdot E_{y,11} + c_{10} \cdot E_{y,10} + Z_{Ot}$	$c_{10}=c_{11}=c_{12}$
Pump 1	$c_{14} \cdot E_{y,14} = c_{13} \cdot E_{y,13} + c_{elec,3} \cdot W_{y,pump1} + Z_{pump1}$	$c_{elec,3}=c_{Ot}$
Condenser 1	$c_{13} \cdot E_{y,13} + c_{29} \cdot E_{y,29} = c_{28} \cdot E_{y,28} + c_{12} \cdot E_{y,12} + Z_{cond1}$	$c_{13}=c_{12}$
Preheater	$c_{w2} \cdot E_{y,w2} + c_{15} \cdot E_{y,15} = c_{w1} \cdot E_{y,w1} + c_{14} \cdot E_{y,14} + Z_{preh}$	$c_{w1}=c_{w2}=0$
Pump 2	$c_9 \cdot E_{y,9} = c_7 \cdot E_{y,7} + c_{elec,2} \cdot W_{y,pump2} + Z_{pump2}$	$c_{elec,2}=c_{Ot}$
Pump 3	$c_8 \cdot E_{y,8} = c_6 \cdot E_{y,6} + c_{elec,3} \cdot W_{y,pump3} + Z_{pump3}$	$c_{elec,3}=c_{Ot}$
Vapor generator 3	$c_{w3} \cdot E_{y,w3} + c_{23} \cdot E_{y,23} = c_{w2} \cdot E_{y,w2} + c_{22} \cdot E_{y,22} + Z_{vg,3}$	$c_{w3}=c_{w2}$
Valve	/	$c_{19}=c_{20}$
Pump 4	$c_{22} \cdot E_{y,22} = c_{18} \cdot E_{y,18} + c_{elec,3} \cdot W_{y,pump4} + Z_{pump4}$	$c_{elec,4}=c_{Ot}$
Condenser 2	$c_{17} \cdot E_{y,17} + c_{31} \cdot E_{y,31} = c_{30} \cdot E_{y,30} + c_{16} \cdot E_{y,16} + Z_{cond2}$	$c_{16}=c_{17}$
Ejector	$c_{16} \cdot E_{y,16} = c_{23} \cdot E_{y,23} + c_{21} \cdot E_{y,21}$	/
Evaporator	$c_{21} \cdot E_{y,21} + c_{25} \cdot E_{y,25} = c_{20} \cdot E_{y,20} + c_{24} \cdot E_{y,24} + Z_{ev}$	$c_{20}=c_{21}$

Table 3 Condition of simulation for the CCP system

Term	Value
Ambient temperature (℃)	20
Ambient pressure (MPa)	0.101

Compressor inlet temperature (℃)	35
BC turbine inlet temperature (℃)	400
BC turbine inlet pressure (MPa)	18
BC turbine outlet pressure (MPa)	8
Inlet temperature at the high-pressure side of ORC turbine (℃)	150
Inlet pressure at the high-pressure side of ORC turbine (MPa)	1.6
Inlet temperature at the low-pressure side of ORC turbine (℃)	100
Inlet pressure at the low-pressure side of ORC turbine (MPa)	1.0
Outlet pressure of pump 1 (MPa)	0.9
Ejector primary inlet pressure (MPa)	0.4
Terminal temperature difference at gas heater outlet (℃)	100
Pinch point temperature difference in vapor generator 1 (℃)	30
Pinch point temperature difference in vapor generator 2 (℃)	30
Pinch point temperature difference in vapor generator 3 (℃)	25
Condensation temperature of condenser 1 (℃)	30
Condensation temperature of condenser 2 (℃)	30
Evaporation temperature of evaporator (℃)	5
Isentropic efficiency of BC turbine (%)	80
Isentropic efficiency of ORC turbine (%)	80
Isentropic efficiency of compressor (%)	80
Isentropic efficiency of pump 1 (%)	75
Isentropic efficiency of pump 2 (%)	75

Isentropic efficiency of pump 3 (%)	75
Inlet temperature of cooling water (℃)	20

Table 4 Main parameters of the engine [8]

Parameters	Value
Power output (kW)	2928
Rotation ($r(min)^{-1}$)	1000
Exhaust gas temperature (℃)	470
Exhaust gas mass flow rate ($kg\ s^{-1}$)	4.35
Temperature of jacket water (℃)	90/79
Mass flow rate of jacket water ($kg\ s^{-1}$)	25

Table 5 Composition of the exhaust gas [8]

Composition	Molecular ($g(mol)^{-1}$)	Fraction (%)
O_2	32.00	9.3
CO_2	44.00	9.1
H_2O	18.01	7.4
N_2	28.01	74.2

Table 6 Parameters for GA

Ranges of the decision variables	Range
BC turbine inlet temperature (℃)	330-440
BC turbine inlet pressure (MPa)	15-20
Inlet temperature at the high-pressure side of ORC turbine (℃)	130-180
Inlet pressure at the high-pressure side of ORC turbine (MPa)	1.4-2

Inlet temperature at the low-pressure side of ORC turbine (℃)	90-150
Inlet pressure at the low-pressure side of ORC turbine (MPa)	0.9-1.3
Ejector primary inlet pressure (MPa)	0.3-1

997 **Table 7** Control parameters of GA

Tuning parameters	Value
Population size	20
Mutation probability	0.01
Crossover probability	0.8
Stop generation	200

998 **Table 8** Single-objective optimization results

Term	Value
BC turbine inlet temperature (℃)	425.457
BC turbine inlet pressure (MPa)	20
Inlet temperature at the high-pressure side of ORC turbine (℃)	144.315
Inlet pressure at the high-pressure side of ORC turbine (MPa)	1.847
Inlet temperature at the low-pressure side of ORC turbine (℃)	100.032
Inlet pressure at the low-pressure side of ORC turbine (MPa)	1.264
Ejector primary inlet pressure (MPa)	0.537
Net power output (kW)	374.37
Cooling capacity (kW)	188.63
Exergy efficiency (%)	37.31
Levelized exergy cost ($ (MWh)$^{-1}$)	53.25

Table B1 Constants for component costs [32]

Constant	Value	Constant	Value	Constant	Value
$B_{1,\mathrm{he}}$	1.63	$K_{3,\mathrm{pump}}$	0.1538	$C_{3,\mathrm{he}}$	0.08183
$B_{2,\mathrm{he}}$	1.66	$K_{1,\mathrm{turb}}$	2.7051	$C_{1,\mathrm{pump}}$	-0.3635
$B_{1,\mathrm{pump}}$	1.89	$K_{2,\mathrm{turb}}$	1.4398	$C_{2,\mathrm{pump}}$	0.3957
$B_{2,\mathrm{pump}}$	1.35	$K_{3,\mathrm{turb}}$	-0.1776	$C_{3,\mathrm{pump}}$	-0.0026
$K_{1,\mathrm{he}}$	4.3247	$K_{1,\mathrm{comp}}$	2.2897	$F_{\mathrm{M,he}}$	1.0
$K_{2,\mathrm{he}}$	-0.3030	$K_{2,\mathrm{comp}}$	1.3604	$F_{\mathrm{BM,turb}}$	3.5
$K_{3,\mathrm{he}}$	0.1634	$K_{3,\mathrm{comp}}$	-0.1027	$F_{\mathrm{BM,comp}}$	2.7
$K_{1,\mathrm{pump}}$	3.3892	$C_{1,\mathrm{he}}$	0.03881	$F_{\mathrm{M,pump}}$	2.2
$K_{2,\mathrm{pump}}$	0.0536	$C_{2,\mathrm{he}}$	-0.11272		

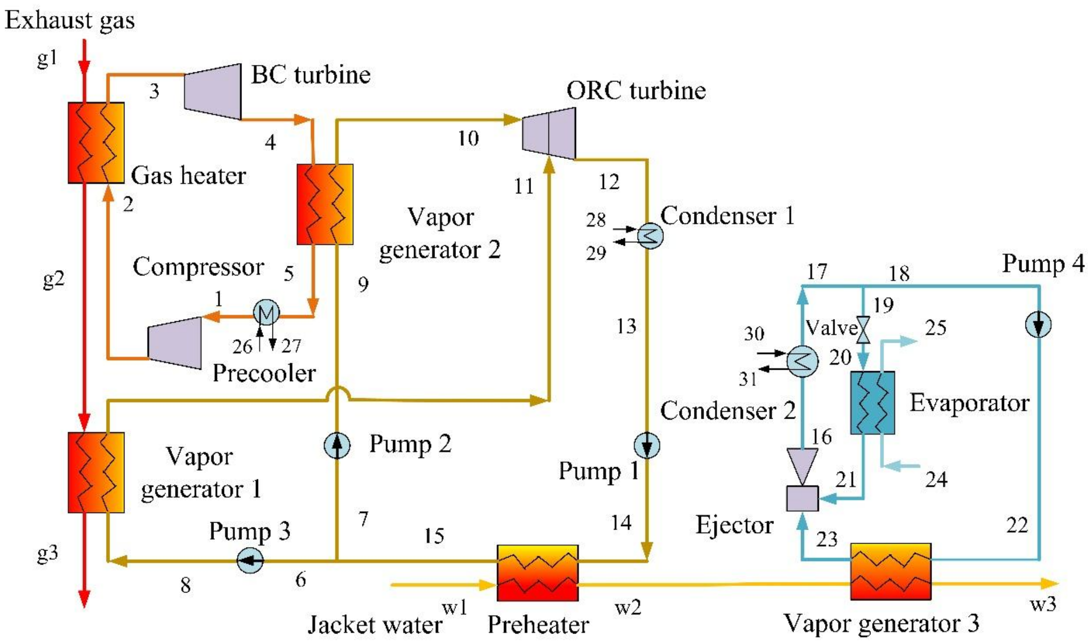

Fig. 1. Schematic diagram of the CCP system

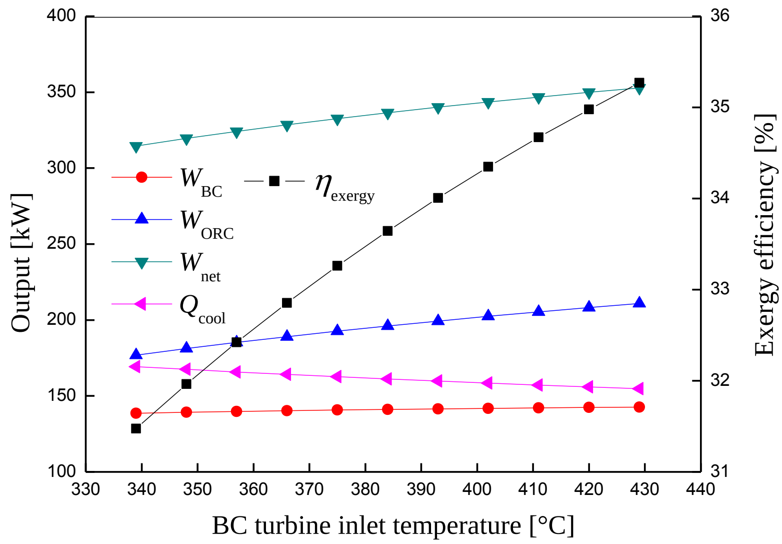

Fig. 2. Influences of BC turbine inlet temperature on the output and the exergy efficiency of the system.

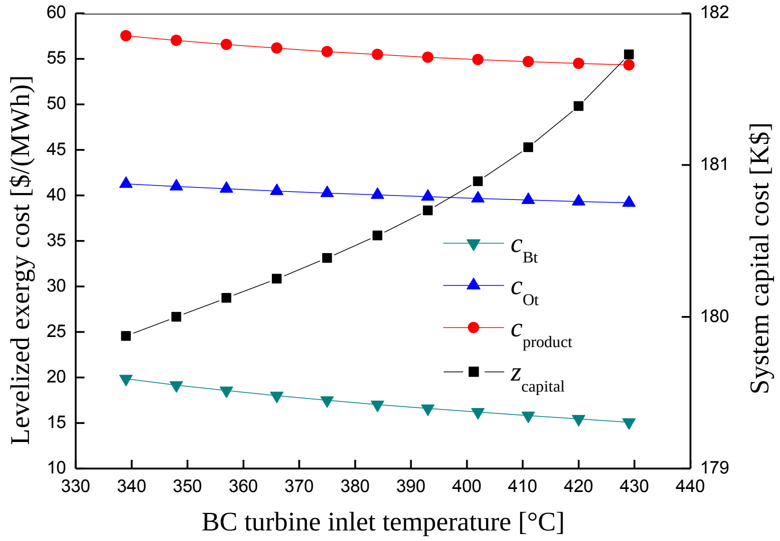

Fig. 3. Influences of BC turbine inlet temperature on the levelized exergy cost and the system capital cost of the system.

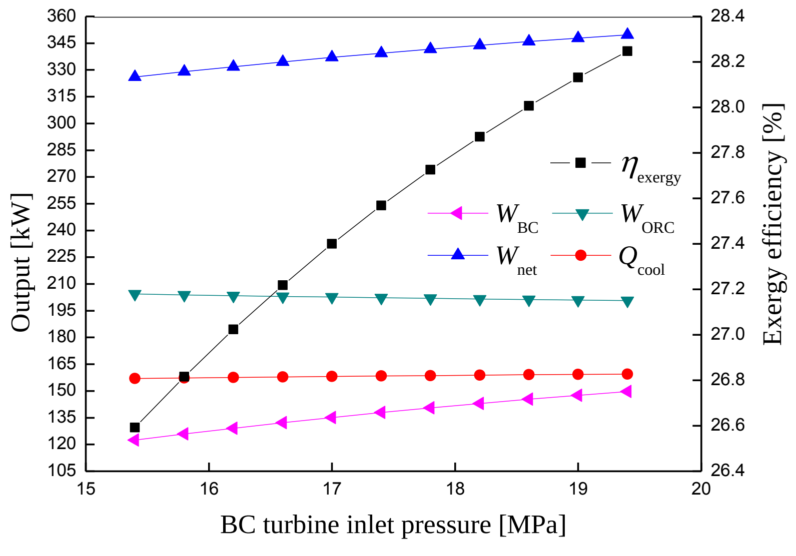

Fig. 4. Influences of BC turbine inlet pressure on the output and the exergy efficiency of the system.

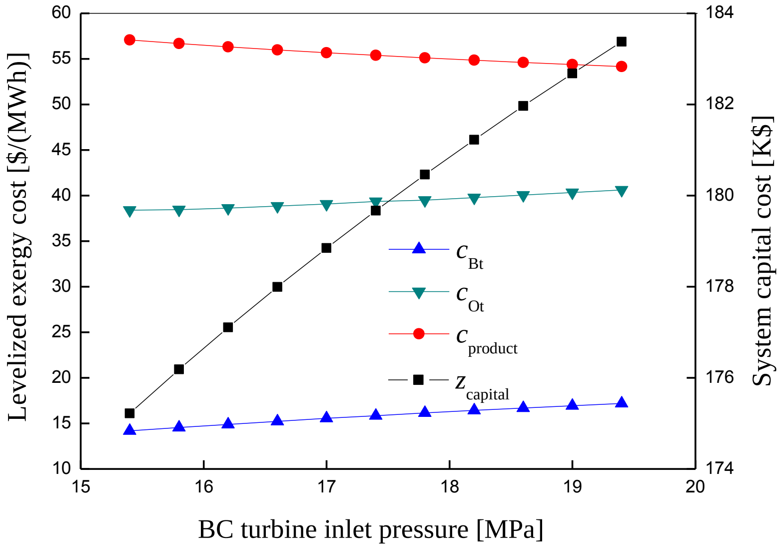

Fig. 5. Influences of BC turbine inlet pressure on the levelized exergy cost and the system capital cost of the system.

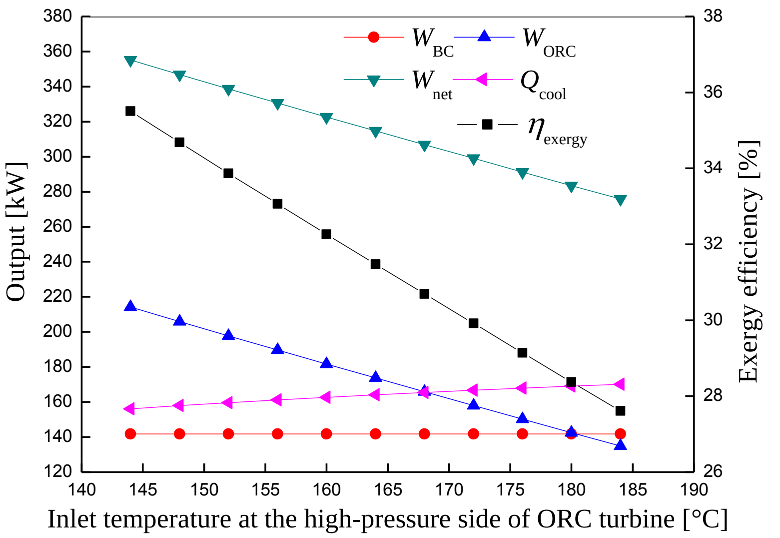

Fig. 6. Influences of inlet temperature at the high-pressure side of ORC turbine on the output and the exergy efficiency of the system.

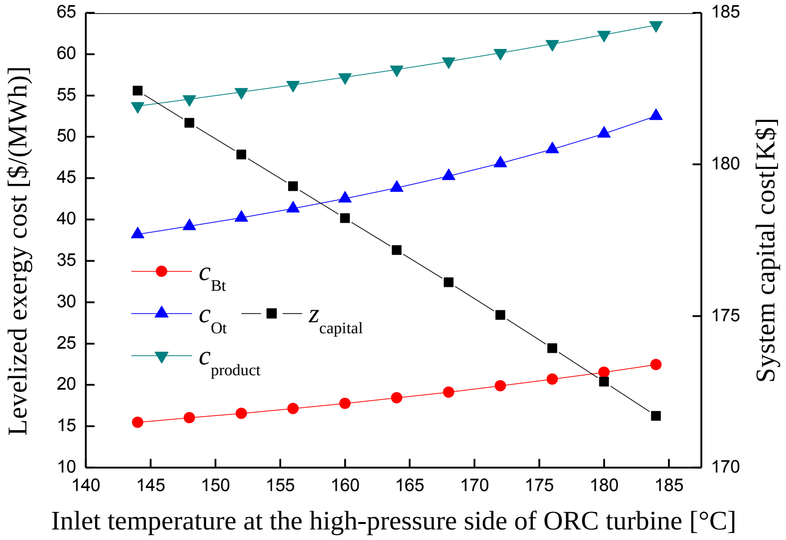

Fig. 7. Influences of inlet temperature at the high-pressure side of ORC turbine on the levelized exergy cost and the system capital cost of the system.

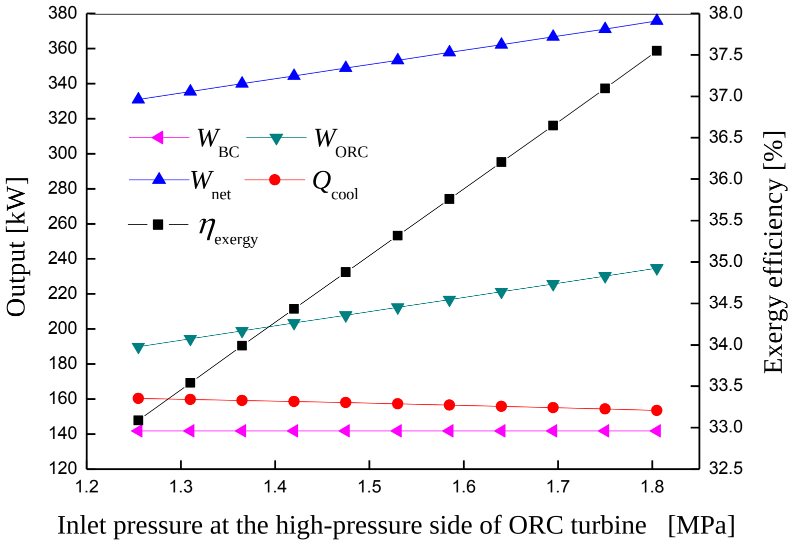

Fig. 8. Influences of inlet pressure at the high-pressure side of ORC turbine on the output and the exergy efficiency of the system.

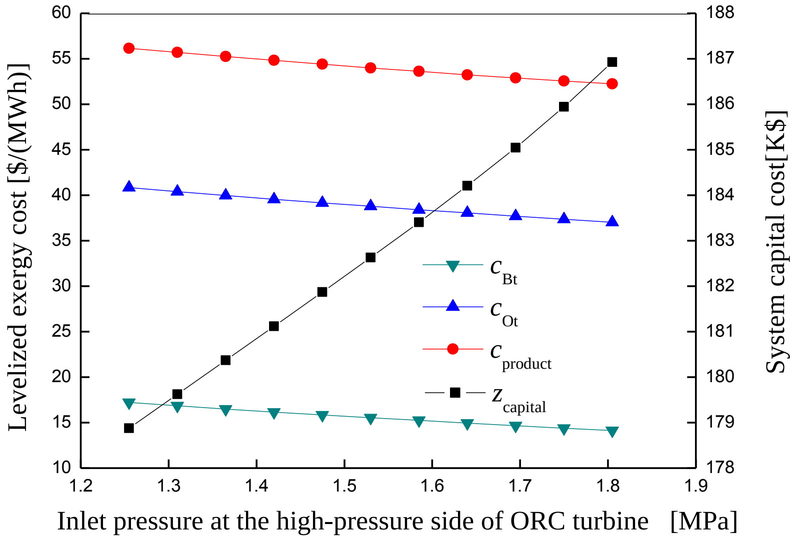

Fig. 9. Influences of inlet pressure at the high-pressure side of ORC turbine on the levelized exergy cost and the system capital cost of the system.

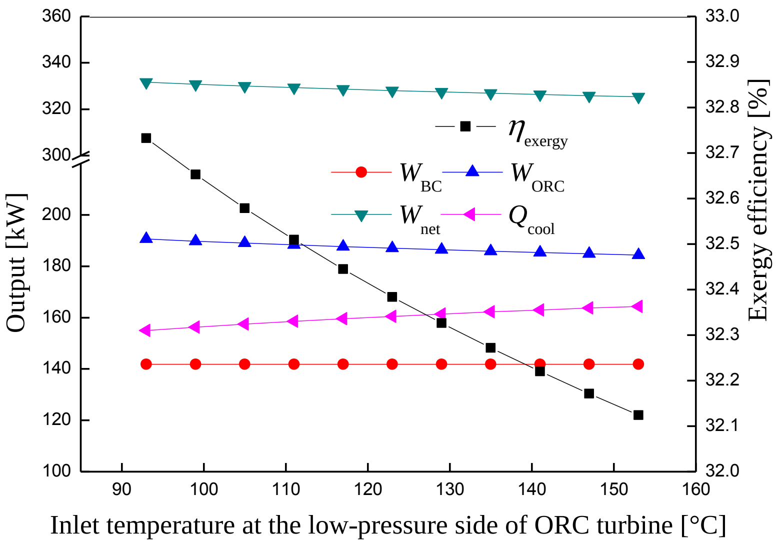

Fig. 10. Influences of inlet temperature at the low-pressure side of ORC turbine on the output and the exergy efficiency of the system.

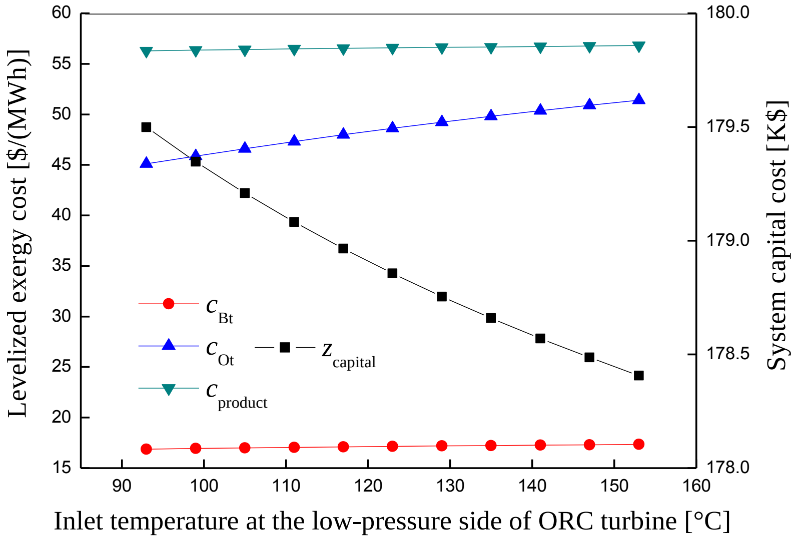

Fig. 11. Influences of inlet temperature at the low-pressure side of ORC turbine on the levelized exergy cost and system capital cost of the system.

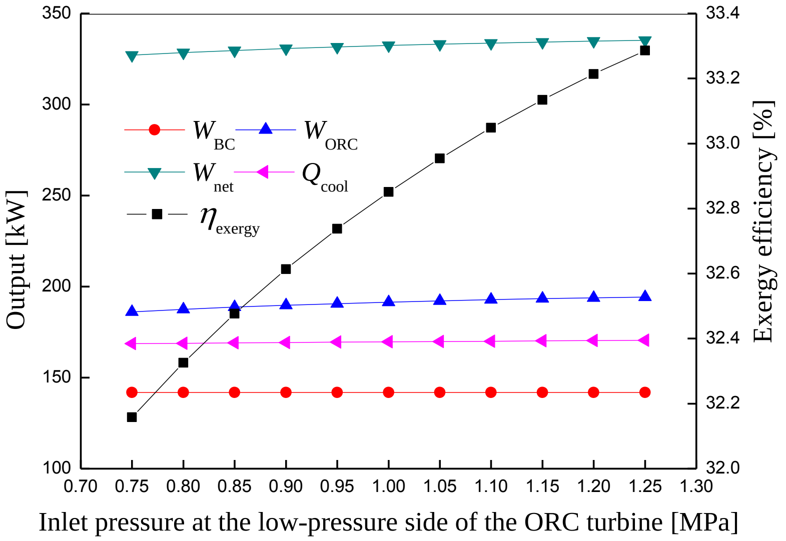

Fig. 12. Influences of inlet pressure at the low-pressure side of ORC turbine on the output and the exergy efficiency of the system.

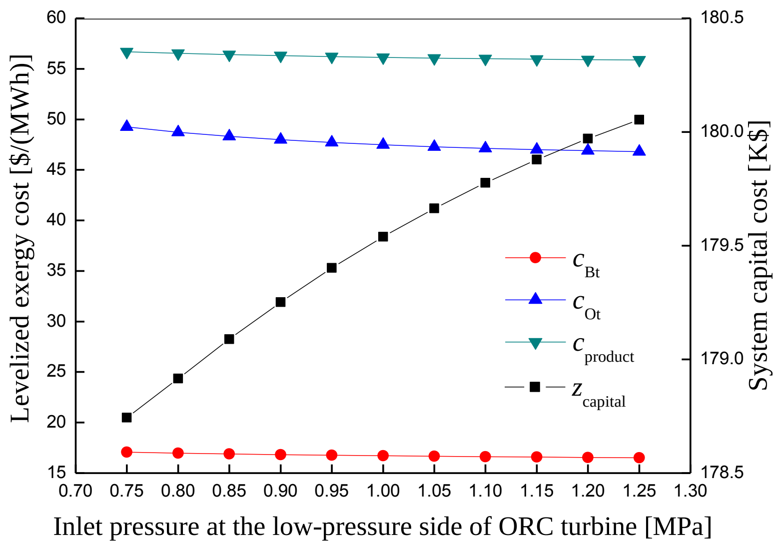

Fig. 13. Influences of the inlet pressure at the low-pressure side of ORC turbine on the levelized exergy cost and system capital cost of the system.

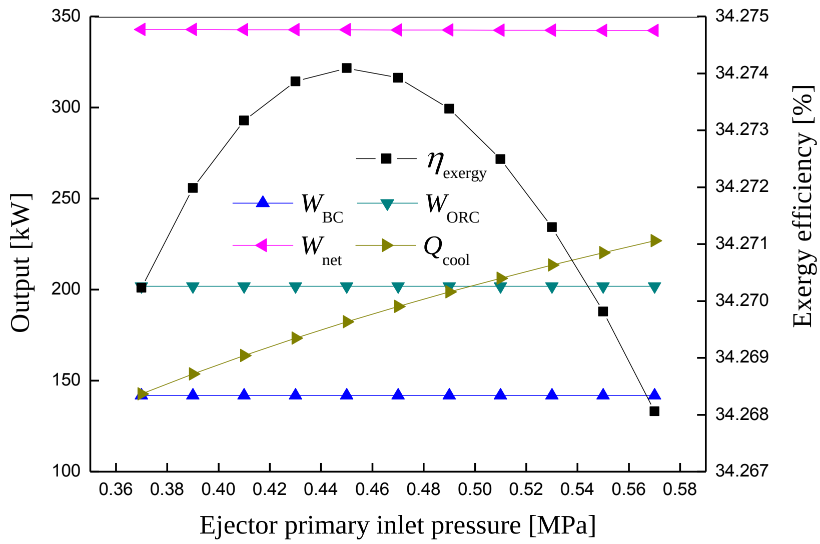

Fig. 14. Influences of ejector primary inlet pressure on the output and the exergy efficiency of the system.

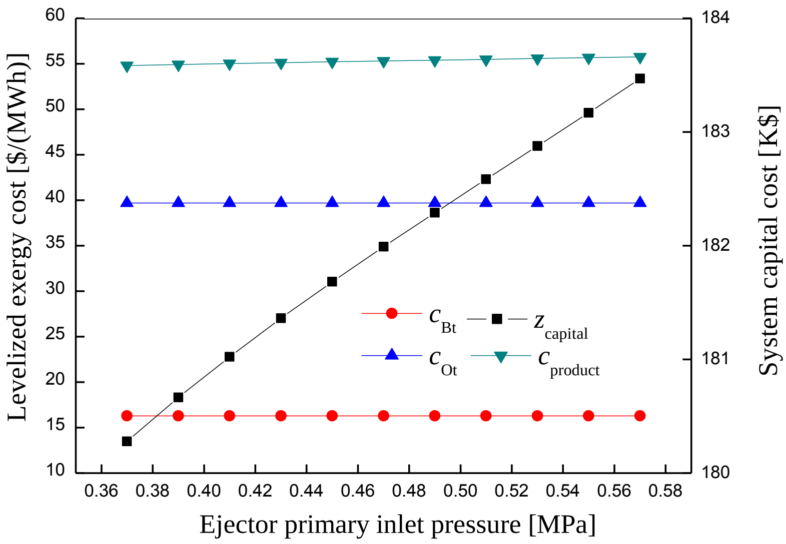

Fig. 15. Influences of ejector primary inlet pressure on the levelized exergy cost and the system capital cost of the system.